
1 This manuscript has been submitted for publication in SEDIMENTARY GEOLOGY
2 and has not yet undergone peer-review. If accepted, the final version of this
3 manuscript will be available via the 'Peer-reviewed Publication DOI' link on the right-
4 hand side of this webpage. Please feel free to contact any of the authors; we
5 welcome feedback

6

7 **Palaeoenvironmental and tectonic significance of Miocene lacustrine and**
8 **palustrine carbonates (Ait Kandoula Formation) in the Ouarzazate Foreland**
9 **Basin, Morocco.**

10 Sarah J. Boulton*¹, Justin H. VanDeVelde¹† and Stephen T. Grimes¹

11 ¹ School of Geography, Earth and Environmental Sciences, University of Plymouth,
12 Drakes' Circus, Plymouth, PL4 8AA, UK

13 ***Corresponding author:** Sarah Boulton sarah.boulton@plymouth.ac.uk

14 † Now at: University of California-Merced, 5200 North Lake Road, Merced, CA
15 95343, USA.

16

17 **Abstract**

18 The Ouarzazate Basin is the southern foreland basin to the High Atlas Mountains in
19 Morocco. The sedimentary fill records a sequence from the Eocene to Pleistocene
20 that records the interplay between tectonics and climate. This study presents the first
21 stable isotope and facies analyses of the Middle to Late Miocene Ait Ibrirn lacustrine
22 Member (Ait Kandoula Formation). These data test whether the basin was internally
23 draining and enable the development of palaeoenvironmental models for the Middle
24 to Late Miocene. Five sedimentary facies of lacustrine and palustrine limestones are
25 interbedded with extensive sequences of palaeosols and fluvial sandstones and
26 conglomerates, often associated with evaporite (gypsum) development. These
27 facies can be divided into two facies associations related to water depth and sub-
28 aerial exposure within the basin. In the Serravalian and Tortonian shallow water
29 successions dominate the stratigraphy, typical of underfilled foreland basin settings.

30 Furthermore, carbonate $\delta^{18}\text{O}$ and $\delta^{13}\text{C}$ isotopes from the sections show covariance
31 confirming that these carbonates were deposited within a hydrologically closed
32 basin. However, late Tortonian to Messinian carbonates do not demonstrate the
33 covariance typical of endorheic basins. Additionally, the facies association indicates
34 the presence of deeper water lake systems demonstrating that the basin was
35 externally draining at this time. These results question the established view of
36 tectonic stagnation in the Late Miocene and suggest that the Cenozoic sediments of
37 the Ouarzazate Basin contain a rich and untapped record of climate change and
38 tectonic evolution on the edge of the Sahara desert.

39 Keywords: palustrine, lacustrine, terrestrial carbonates, stable isotopes, Morocco.

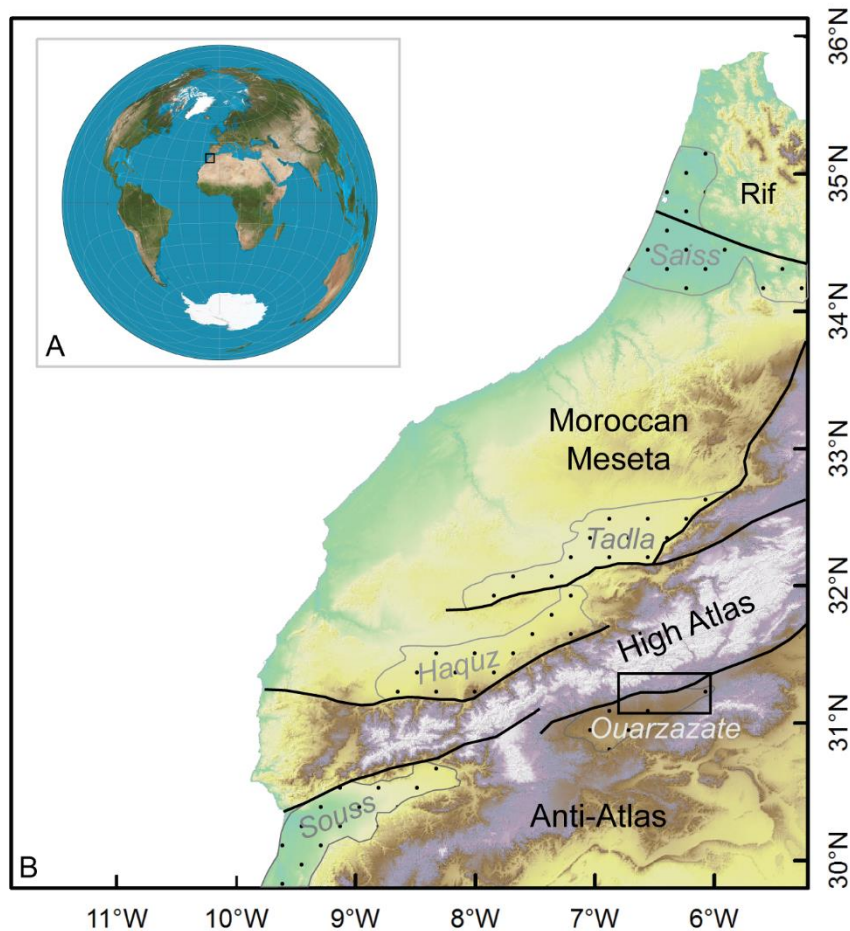
40

41 **INTRODUCTION**

42 Terrestrial carbonates have long been recognised as being excellent archives of
43 climatic, environmental and tectonic information. Terrestrial carbonates can be
44 found in extensional, compressional and cratonic settings and form in a wide variety
45 of conditions from deep and shallow permanent lakes, palustrine conditions, to
46 fluvially dominated plains. As a result the boundaries between different terrestrial
47 sub-environments are not always clear (Alonso-Zarza, 2003) especially when there
48 is no clear link between lake size, salinity, and climatic humidity (Herdendorf, 1984).
49 This is especially true in semi-arid and arid environments where sub-aerial exposure
50 and evaporation are common, which can result in pedogenic overprinting of
51 previously deposited lacustrine carbonates forming the palustrine facies
52 characteristic of seasonal wetlands (Platt and Wright, 1992; Wright and Platt, 1995).
53 However, detailed sedimentology and petrography (i.e., Freytet and Verrecchia,
54 2002), combined with a robust stratigraphic framework (Bohacs et al., 2000) can
55 allow the reconstruction of the morphology and type of palaeolakes. In addition, the
56 geochemistry of primary carbonates can record the interplay between autogenic
57 factors such as basin hydrology and biogenic productivity and allogenic effects of
58 climate change, tectonics and drainage network evolution (i.e., Talbot, 1990; Talbot
59 and Kelts, 1990; Valero-Garcés et al., 1995). Thus, providing records of terrestrial
60 paleoenvironmental changes that occurred through the evolution of lake systems.

61 In foreland basin settings, available accommodation space is controlled by the
62 competition between subsidence, driven by loading, and uplift, resulting from
63 thickening and rebound (DeCelles and Giles, 1996). While sediment supply reflects
64 climate, uplift rate and river catchment size (Allen et al., 2013). Thus the balance
65 between subsidence and sediment flux results in underfilling, filling or overfilling of
66 the available accommodation space in basin and is preserved in the sedimentary
67 record of the basin through facies patterns and grainsize trends (i.e., Duller et al.,
68 2010; Whittaker, 2011; Parsons et al., 2012). Therefore, lacustrine-paulstrine
69 wetlands in foreland basins can be sensitive recorders not only of
70 palaeoenvironments within the basin but also reflect the uplift and erosion of the
71 adjacent mountain front and the evolution of foreland basin drainage configurations.

72 Here, Miocene limestones from the Ouarzazate Foreland Basin of Morocco
73 (Fig. 1) are described using standard facies descriptions for the first time. In addition,
74 the first stable isotope data from these sediments are presented challenging the long
75 held hypothesis that the palustro-lacustrine sediments were deposited entirely within
76 a closed basin environment (Görlner et al., 1988; El Harfi et al., 2001). These data not
77 only provide new insights into the palaeoenvironments of the Ouarzazate Basin in
78 the Middle to Late Miocene but also have implications for our understanding of the
79 evolution of the adjacent High Atlas Mountains.



80

81 *Figure 1. 30 m SRTM digital elevation model of Morocco showing the main tectonic units*
82 *and Cenozoic sedimentary basins (grey text). Box indicates the location of figure 2. Globe*
83 *inset shows the location of the DEM in Africa.*

84

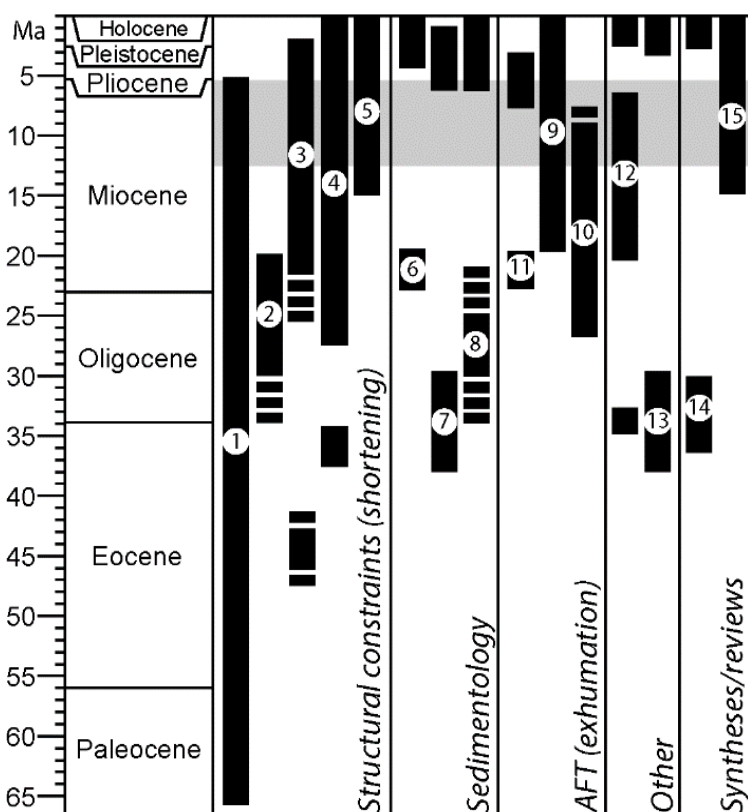
85 **GEOLOGICAL BACKGROUND AND STRATIGRAPHIC FRAMEWORK**

86 The High Atlas Mountains are a ~ W – E trending intracontinental mountain
87 belt formed through the inversion of a Mesozoic rift system owing to N-S directed
88 compression in the Cenozoic (e.g., Jacobshagen et al., 1988; Frizon de Lamotte,
89 2000). The South Atlas Fault (SAF) and the North Atlas Fault (NAF) form the
90 southern and northern margins of the High Atlas, respectively (Fig. 1), and the Anti-
91 Atlas Mountains to the south form the forebulge to the southern foreland basins.
92 Mountain building is thought to have commenced in the Eocene, although the exact
93 timing of deformation is still a matter of debate owing to the range of evidence used
94 to investigate the development of the orogeny (Fig. 2). Some authors advocate
95 multiple phases of uplift primarily based upon sedimentological observations (i.e.,

96 Gorler et al., 1988; Frizon de Lamotte et al., 2000; El Harfi et al., 2001). While
 97 others propose continuous deformation from the Oligo-Miocene onward (i.e., Babault
 98 et al., 2008; Teson and Teixell, 2008; Balestrieri et al., 2009) based upon structural
 99 relationships and apatite fission track data.

100 South of the High Atlas, two foreland basins have developed during the
 101 Cenozoic as a result of lithospheric flexure in response to crustal loading
 102 (Beauchamp et al., 1999). These are the Souss Basin in the west and the
 103 Ouarzazate Basin in the east, separated by a topographic high of the Siroua Plateau
 104 (Fig. 1). The Ouarzazate Basin fill is ~ 1 km thick, composed of Oligocene to
 105 Quaternary alluvial, fluvial and lacustrine sediments (e.g., Fraissinet et al., 1988;
 106 Görler et al., 1988; El Harfi et al., 2001; Teson and Teixell, 2006; Teson et al., 2010).
 107 To the north of the Ouarzazate Basin, in the High-Atlas fold and thrust belt that forms
 108 the southern margin of the High Atlas Mountains, the Aït Kandoula and Aït Seddrat
 109 piggy-back basins also contain continental sequences (Fig. 3a). The syntectonic
 110 sediments deposited in these basins preserve a key record of the evolution of the
 111 High Atlas system.

112



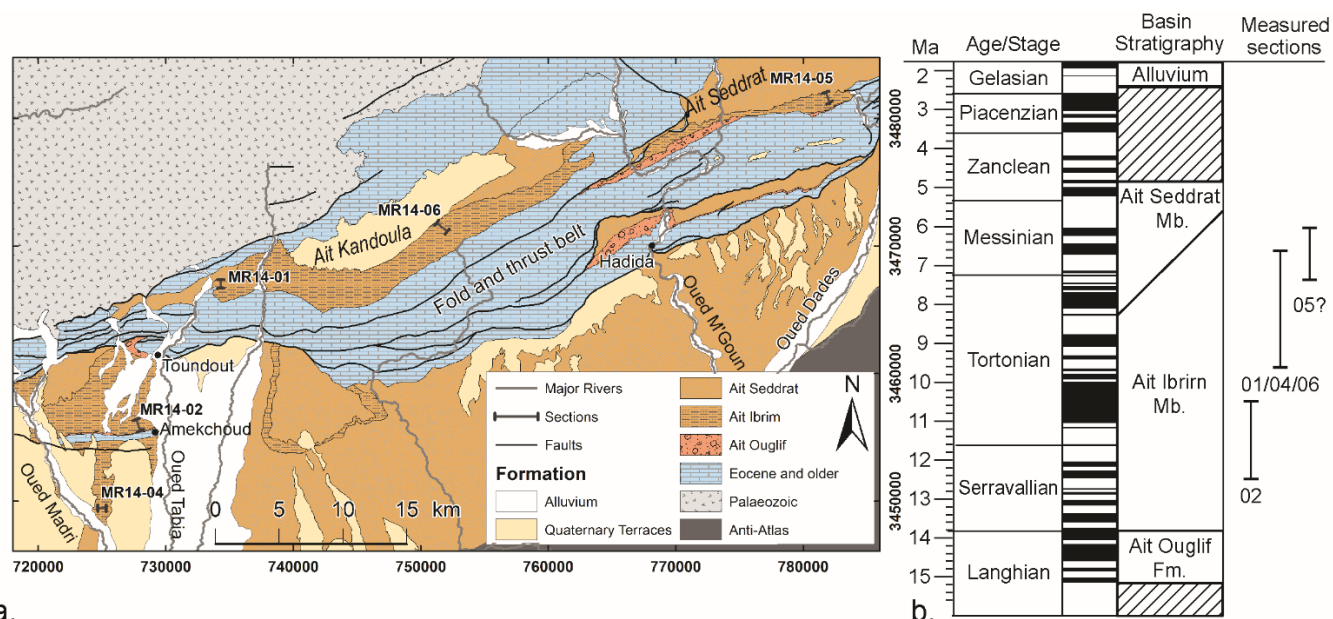
113

114 *Figure 2. Timing of uplift of the High Atlas derived from different lines of evidence: 1)*
115 *Faissinet et al. (1988); 2) Beauchamp et al (1999); 3) Teson & Teixell (2008); 4) Teson et al.*
116 *(2010); 5) Pastor et al. (2012); 6) Görler et al., (1998); 7) El Harfi et al. (2001; 2006); 8)*
117 *Babault et al. (2008); 9) Barbero et al. (2007); 10) Missenard et al. (2008); 11) Balestrieri et*
118 *al. (2009); 12) Missenard et al. (2006); 13) Frizon de Lamotte et al. (2000; 2009); 15) Gomez*
119 *et al. (2000). Grey box indicates timespan of this study. AFT – Apatite Fission track.*

120

121 Early studies by Görler et al. (1988) and Fraissinet et al. (1988) recognised in
122 these basins two main Cenozoic units, the Hadida and Aït Kandoula formations,
123 which were deposited unconformably over older stratigraphy. The Hadida
124 Formation, was interpreted by Görler et al. (1988) as being deposited in proximal
125 braided rivers and alluvial fans during the Early Oligocene to Early Miocene. While,
126 the overlying Aït Kandoula Formation was subdivided into three lithostratigraphic
127 units; an 'alluvial base member', the 'lacustrine member' and the 'alluvial top
128 member' loosely dated as being Early Miocene to Pliocene in age (Görler et al.,
129 1988). Görler et al. (1988) described the lacustrine member as being a sequence of
130 mudstones with various interbeds of conglomerates, limestones and gypsum, which
131 they interpreted as representing environmental changes between freshwater lakes
132 and perennial saline lakes in a hydrologically closed basin.

133 However, issues with dating and lateral continuity of units led El Harfi et al.
134 (2001) to formally (re)define the Cenozoic units of the Ouarzazate and Sub-Atlas
135 basins. They described an Upper Eocene Hadida Formation and Aït Arbi Formation
136 (previously the one formation), an Oligocene Aït Ouglif Formation (c.f., alluvial base
137 member of Görler et al., 1988), and the Mio-Pliocene Aït Kandoula Formation. The
138 Aït Kandoula Formation consisted of the previous 'lacustrine member' and 'alluvial
139 top member', which El Harfi et al (2001) recognised as unconformably overlying the
140 Palaeogene stratigraphy. Teson and Teixell (2008) have subsequently formally
141 subdivided the Aït Kandoula Formation into the lower Aït Ibrirn Member
142 (lacustrine/palustrine environments) and the upper Aït Seddrat Member of alluvial
143 fan conglomerates. Although El Harfi et al., (2001) and Teson and Teixell (2008)
144 established a new stratigraphic framework (Fig. 3b) they did not substantially
145 advance the sedimentology and palaeoenvironmental interpretation of the Aït Ibrirn
146 member from that previously described by Görler et al. (1988).



a.

147

148 *Figure 3 A) Geological map of the study area [modified from Teson and Teixell (2008) and*
 149 *Teson et al. (2010)], showing the location of the sections described herein. B) Inferred*
 150 *stratigraphic age and extent of the measured sections (01, 02 etc.) and lithostratigraphic*
 151 *units of the Ouarzazate basin (El Harfi et al., 2001; Teson et al., 2010) against the geological*
 152 *timescale and magnetic polarity of Gradstein et al., (2012).*

153

154 Discoveries of mammalian fauna (Jaeger, 1977; Görler et al., 1998; Benammi et al.,
 155 1995; 1996; Remy and Benammi, 2006; Zouhri et al., 2012), ash layers (Benammi et
 156 al., 1996) and magnetostratigraphic investigations in the Aït Kandoula (Benammi et
 157 al., 1996; Benammi and Jaeger, 2001) and Ouarzazate Basins (Teson et al., 2010)
 158 have continuously refined the dating of the Cenozoic sequence. The current
 159 constraints suggest that the Hadida and Aït Arbi formations are likely Lutetian to
 160 Bartonian in age, the overlying Aït Ouglif Formation dates to the Langhian and the
 161 Aït Kandoula Formation was deposited during the Serravallian to Messinian (Fig. 3b;
 162 ~13.5 – 5 Ma: Teson et al., 2010).

163 At the present, the lacustrine deposits in the Aït Kandoula and Aït Seddrat basins
 164 are located at higher topographic elevations than the locations sampled in the main
 165 Ouarzazate Basin (Fig. 3), yet structural analyses of the fold and thrust belt indicate
 166 that range front thrusting activated during the deposition of the Aït Ibrim Member.
 167 (Teson & Teixell, 2008). While tectonic deformation may have resulted in some
 168 compartmentalization of lacustrine depo-centres, it is not clear if there were

169 substantial changes in elevation between lakes in different parts of the foreland
170 basin system. The main phase of thrusting seems to have occurred during the
171 deposition of the subsequent Ait Seddrat Member (Teson & Teixell, 2008), leading to
172 the suggestion that the lakes could have been connected prior to that time (Görler et
173 al., 1998).

174

175 **METHODS**

176 Field stratigraphic and petrographic observations of the Ait Ibrirn Member were
177 accomplished by sedimentary logging of five key sections, which form a vertical
178 transect through the member. Petrographic analysis of 28 thin sections from
179 carbonate beds were used to identify carbonate microfacies based upon
180 sedimentary, petrographic and textural features (Dunham, 1962; Flugel, 2004).
181 These analyses were supplemented by staining of selected thin sections with
182 Alizarin Red S and potassium ferricyanide to identify dolomite, and cathode
183 luminescence was utilised to identify different phases of micrite formation. Cathode
184 luminescence was undertaken at the University of Plymouth using a CITL cold
185 cathode luminescence Mk5-2 microscope with operating conditions of < 10 kV and <
186 200 μ A.

187 Carbonate microsamples (~300 ug) for isotopic analysis were collected from
188 114 slabbed and polished hand samples, using an electric drill under a binocular
189 microscope. Sampling focused on the micritic matrix of each sample, avoiding
190 diagenetic spar, intraclasts, and biogenic material, such as gastropod shells, to avoid
191 difficulties in the interpretation of the isotope results due to alteration, transport, or
192 biological factors. Microsamples were subsequently sealed in individual reaction
193 vials, flushed with helium, and digested with phosphoric acid at 90 °C. Evolved CO₂
194 was then analysed on a VG Optima isotope ratio mass spectrometer coupled to a
195 Multiprep Automated Carbonate System at the University of Plymouth. Replicate
196 analyses of NBS-19 and internal laboratory standards yielded precisions of ± 0.3 ‰
197 or better for $\delta^{13}\text{C}$ and $\delta^{18}\text{O}$. Both isotope ratios are reported relative to Vienna
198 PeeDee Belemnite (VPDB).

199

200 **STRATIGRAPHIC CORRELATION**

201 For this study, five representative sections of the Aït Ibrirn Member (Fig. 3) were
202 selected owing to the existence of previous age constraints (sections 1, 2, 6) or by
203 being located nearby allowing an approximate stratigraphic correlation to previously
204 described localities (Benammi et al., 1996; Benammi and Jaeger, 2001; Teson et al.,
205 2010). In addition, the sections provide a vertical sequence through the Middle to
206 Late Miocene and a lateral sequence west to east through the Ouarzazate, Aït
207 Kandoula and Aït Seddrat Basins allowing the evaluation of palaeoenvironmental
208 trends in time and space.

209 Sections 2 and 4 are from the northern and southern limb of the Amekchoud
210 anticline, respectively (Fig. 3a). Existing dating (Teson et al., 2010) of Section 2
211 allows us to assign an age to the section measured here as ~12.5 – 10 Ma (Fig. 3b).
212 Section 4 has not been previously described and along strike correlations show that
213 section 4 is stratigraphically higher than section 2, suggesting a possible middle to
214 late Tortonian age for this section. Sections 1 and 6 are located within the Aït
215 Kandoula Basin (Fig. 3a) and form part of a continuous sequence of lacustrine
216 sediments that span > 5 Ma (Benammi et al., 1996). Section 6, located in the centre
217 of the basin, correlates to part of Benammi et al.'s (1996) Afoud section which has
218 been dated to the Tortonian and Messinian (~ 10 – 5 Ma). Whereas, section 1 is
219 equivalent to Benammi et al.'s (1996) Oued Tabia section; therefore, this section is
220 probably Tortonian in age (~ 10 - 7 Ma). Section 5 is located in the adjacent Aït
221 Seddrat Basin; although no age constraints are available for this section,
222 stratigraphic similarities to the Oued Tabia section suggests that this section could
223 have also been deposited during the same time interval.

224

225 **RESULTS**

226 **Sedimentary facies description**

227 Fifteen sedimentary facies have been identified in the studied exposures.
228 Summary sedimentary descriptions of the facies are given in Table 1, with facies
229 abbreviations following convention with G for conglomerates, S for sandstones and
230 M for mudstones and siltstones, and L for limestones.

231

232 *Carbonate facies field description*

233 In the field, the carbonate beds are lime mudstones or wackestones, rich in
234 fragmentary bioclastic material and whole gastropods. Bed thickness is variable from
235 1.0 ± 0.2 m to < 0.1 m in thickness, the thinner beds are often laterally discontinuous,
236 while bed boundaries are sharp and conformable. Sedimentary structures are
237 generally rare but some horizons do exhibit wavy and undulating lamination and
238 many beds have a rubbly texture.

239

240 *Carbonate microfacies analysis*

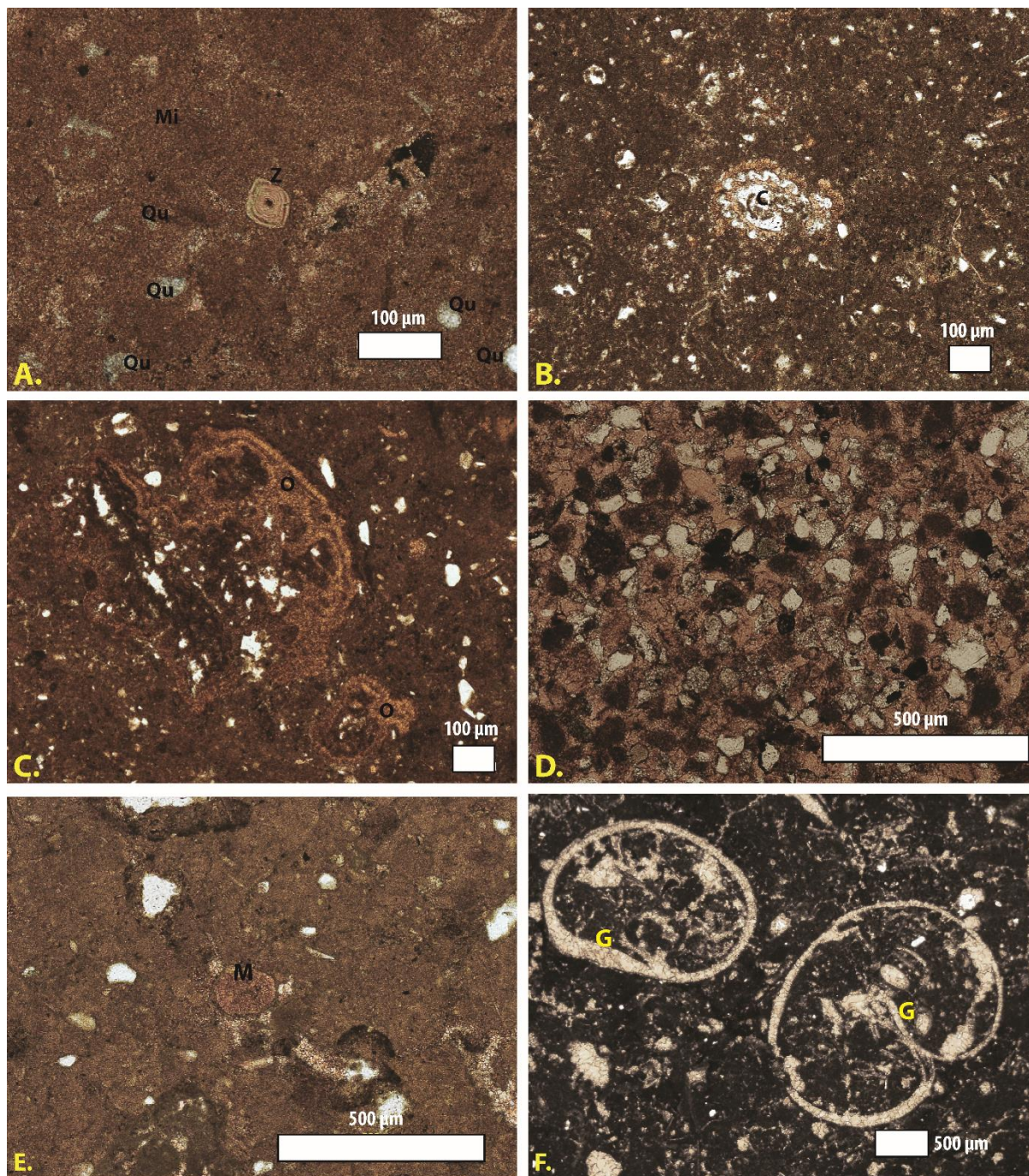
241 Five carbonate microfacies have been identified from detailed petrographic analysis
242 of 18 samples taken from the logged sections, to give greater insight into the
243 carbonate depositional environments. This analysis shows that mudstones are the
244 most common microfacies (and are volumetrically underrepresented in the thin-
245 section analysis as the coarser-grained samples were preferentially selected for
246 further study), followed by wackestones with a variable bioclastic component.
247 Microfacies have been characterised using Flugel's (2004) lacustrine microfacies
248 (LMF) criteria. The majority of the samples show evidence for post-depositional
249 pedogenic alteration consistent with palustrine environments.

250

251 *1. Lime Mudstones/fossiliferous micrite with pedogenic development (LMF1)*

252 This microfacies is composed of a dense micrite matrix exhibiting glaebule (i.e.,
253 irregular masses of secondary micrite) development with some circumgranular
254 cracking around the incipient nodules. The primary micrite contains a small and
255 variable bioclastic component composed primarily of fragmentary material, such as
256 ostracods, bivalves and charophytes. Additionally, there are masses of prismatic
257 sparite crystals likely to be *Microcodium* aggregates. This microfacies also contains
258 a minor siliciclastic component composed of silt-sized ($< 100 \mu\text{m}$), sub-angular to
259 sub-rounded, monocrystalline quartz grains of a detrital origin.

260 Porosity is variable and characterised either by irregular open pores or by lenticular
261 (moldic porosity) holes. Microcrystalline spar and coarser sparite partially infills open
262 porosity and some pore spaces have a gravity fill of micrite.



263
264 *Figure 4. Photomicrographs of the main microfacies all in plane polarised light (PPL) except A in*
265 *cross-polarised light; a) lime mudstone (Mi – micrite) with small quartz clasts (Qu) and zoned grains of*
266 *calcite pseudomorphic after dolomite or gypsum (Z) from section 01; b) example of charophytic*
267 *wackestone facies (C – charophyte) and c) encrusting algal nodule (oncolite – O) from 04; d) Siltstone*

268 with carbonate cement from section MR05; e) lime mudstone containing a spheroidal aggregate of
269 *Microcodium* (M) and f) example of gastropod (G) wackestone from section MR06.

270

271 The original lime mudstone facies is indicative of deposition through settling from
272 suspension, where the micrite likely originated from either cyanobacterial or algal
273 blooms or from abrasion of limestones (Flügel, 2004). This facies is found in deeper
274 protected parts of lacustrine systems as well as in shallower water areas. The
275 samples studied here are typical of lacustrine carbonates that were affected by later
276 pedogenesis and calichefication typical of palustrine environments. Circumgranular
277 cracking occurs when the sediments are subjected to seasonal wetting and drying
278 cycles, while the presence of *Microcodium* and irregular pore space indicates root
279 activity within the sediment (Wright et al., 1995). By contrast, lenticular (moldic)
280 porosity could indicate where evaporitic crystals have been removed, supported by
281 the presence of rare rhombic zoned calcite crystals that are possibly pseudomorphs
282 after dolomite or gypsum (Fig. 4a).

283

284 2. *Densely packed peloidal wackestone (LMF 5)*

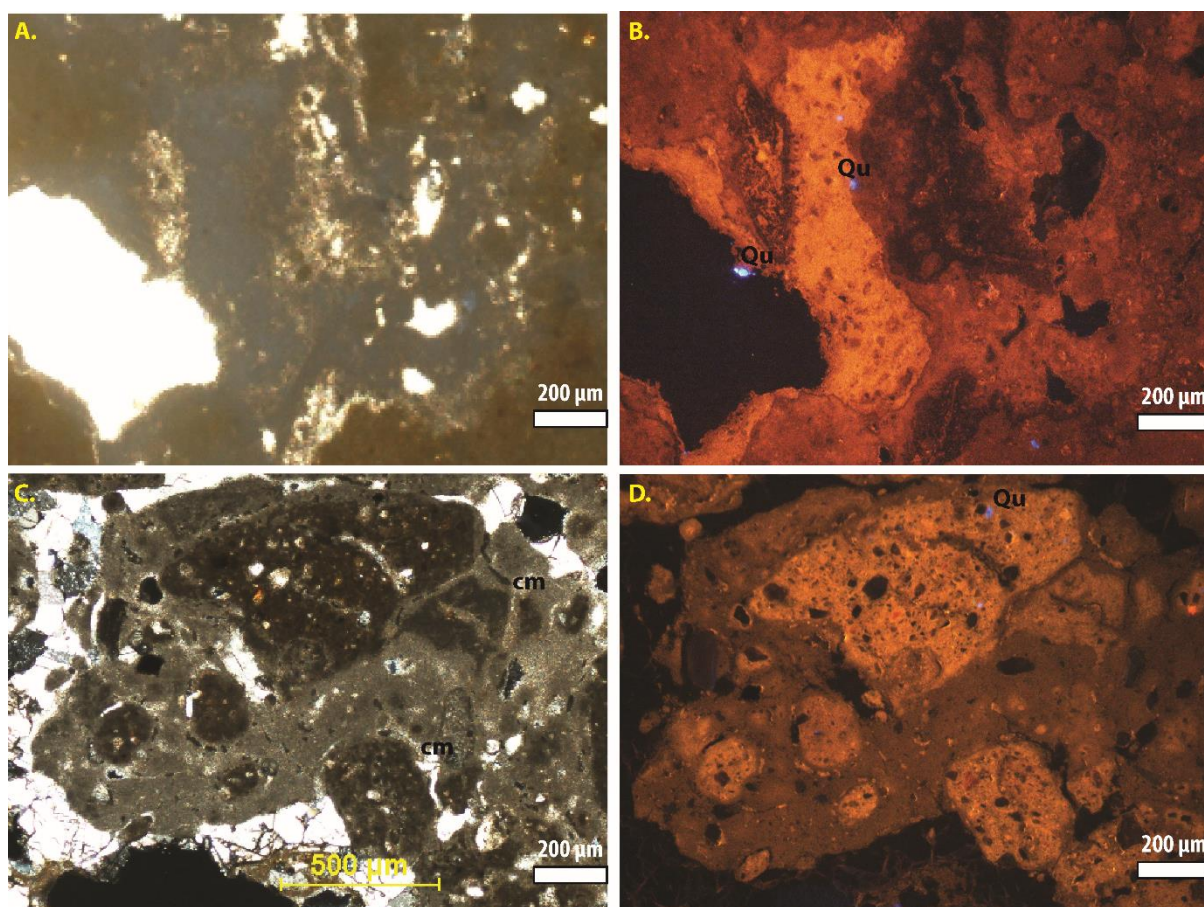
285 This microfacies is composed of a nodular, peloidal micrite matrix with some
286 recrystallisation to microspar. There is a detrital quartz component and fragmentary
287 bioclasts of ostracods, gastropods, charophytes, and algal crusts. Sparite variably
288 infills the original irregular porosity, rarely some infills have a lens of opaque minerals
289 at the base forming a gravitational infill. As many of these infilled pore spaces have
290 flat floors these can be described as fenestrae.

291 The presence of micrite peloids and fragmentary fossil material indicates that this
292 facies was deposited as the result of current reworking in shallow water, probably
293 near the lake shoreline. This is supported by the presence of fragmentary algal mat
294 material that forms on the sediment surface within the photic zone (Freytet &
295 Verrecchia, 2002). Peloids are potentially also the result of reworking of primary
296 precipitates or faecal pellets (Burne and Ferguson, 1983). The open-space
297 structures maybe the result of subsequent bioturbation, sub-aerial dissolution
298 (Flügel, 2004) or be part of the original algal mat structure.

299

300 3. *Charophycean wackestones (LMF 7) with pedogenic development*

301 This microfacies consists of a dense micritic matrix with variable nodule (glaebule)
 302 development with occasional circumgranular cracks beginning to form where nodule
 303 development is the most advanced (Fig. 5). There is minor recrystallisation to
 304 microspar but generally little sparite formation. Charophytes (Fig. 4b) form the most
 305 significant bioclastic component along with calcispheres (probably also charophytic
 306 in origin), fragmentary gastropods, ostracods and bivalves. In addition, laminar algal
 307 material (Fig. 4c) and *Microcodium* are present. There is a detrital siliciclastic
 308 component mainly composed of sub-angular to sub-rounded monocrystalline quartz
 309 grains (>80%), but also polycrystalline quartz, opaque minerals and lithic fragments
 310 are variably present. In addition, there are rare glauconite grains and zoned
 311 euhedral calcite crystals.



312

313 *Figure 5. Comparison of PPL photomicrographs (left) and catholuminescence images (right) of*
 314 *sections 01 and 06. A) and B); Section 01 showing variable luminescence of micrite cement. Note*

315 quartz (Qu) grains with strong blue luminescence. C) and D) from 06 variable luminescence of
316 glaebules with stronger (higher Mg+) in core of the nodules and lower luminescence on the outer
317 areas, also note circumgranular (cm) crack development now infilled with sparite.

318 Charophytes are a type of green algal that inhabit freshwater and brackish
319 environments and are highly characteristic of low energy, shallow water, lacustrine
320 environments (i.e., Platt and Wright, 1991). Combined with the presence of
321 ostracods and encrusting algal material this facies is characteristic of the shoreline
322 region of many lakes (Flugel, 2004).

323 The primary sedimentary fabric is overprinted by secondary features characteristic of
324 caliche development, including dense micrite/glaebules, intergranular cracking, and
325 *Microcodium* aggregates, indicating subaerial exposure and pedogenesis after
326 deposition. *Microcodium* are calcified root cells and indicate that root activity had an
327 important role to play in the secondary alteration of these sediments (Wright et al.,
328 1995).

329

330 4. *Gastropod Wackestone and Packstone (LMF8)*

331 This microfacies is characterised by whole gastropods (Fig. 4f) and well-preserved
332 charophytes (mostly oogonia but some stem material is also present), with
333 fragmentary bioclastic material mostly derived from ostracods and
334 bivalves/gastropods. There is some primary porosity in shell cavities but otherwise
335 lacks other pore space in the micrite matrix, which is fairly texturally uniform but does
336 contain rare silt-sized quartz grains. There is some recrystallisation of shelly
337 material to sparite and some micrite to microspar. The micrite matrix also exhibits
338 minor glaebule development with associated cracking in some areas.

339 The bioclastic component of this microfacies is consistent with shallow water
340 lacustrine deposition and is similar to the Charophycean wackestone but with a
341 much higher gastropod fauna suggesting more permanent water conditions (i.e.,
342 Burne and Ferguson, 1983).

343

344 5. *Carbonate cemented siltstone.*

345 This facies is a siltstone with ~ 70 % clasts and 30 % cement (Fig. 4d). The clasts
346 are either rounded micrite pellets or angular to sub-rounded lithic clasts dominated
347 by monocrystalline quartz (75-80%) and polycrystalline quartz ($\leq 16\%$) with minor
348 opaque minerals (1-3 %) and rare glauconite ($\leq 1\%$). The cement is sparite, infilling
349 the space around the grains, in places there are spar-filled areas with floating clasts
350 resulting in a poikiliptic texture.

351 This facies is interpreted as the calcrete K-horizon. The sparite cement is consistent
352 with alpha microfabrics dominated by non-biogenic features (Wright, 1990)
353 characteristic of palaeosols in arid or semi-arid environments.

354

355 *Summary of carbonate facies*

356 The carbonate beds were deposited across a range of very shallow/intermittently
357 inundated environments to slightly deeper water lake environments. The presence of
358 abundant charophytic material is indicative of low-energy shallow water conditions
359 (Platt and Wright, 1991; Flugel, 2004) and along with the presence of ostracods, is
360 characteristic of freshwater or brackish environments. Slightly deeper water facies
361 show evidence of the reworking of bioclastic material and the addition of
362 allocthonous lithic and fine-grained organic matter. While shallow water facies are
363 coarser-grained and contain material sourced from algal mats; seen in the field as
364 irregular laminations. All carbonate facies have evidence of secondary nodule
365 development, dissolution textures or root traces due to subaerial exposure and
366 vegetation growth after deposition leading to the formation of typical palustrine
367 limestone features.

368

369 *Siliciclastic and Sulphate Facies*

370 *Grey to black mudstones and marls (facies M and Ma)* are generally massive but
371 rarely can exhibit parallel lamination. Fragmentary fossil material is present,
372 especially in the darker sediments. These very fine-grained sediments represent
373 settling from suspension in lacustrine depocentres. The black mudstone indicates

374 enrichment in organic carbon and possible low oxygen conditions within the
375 waterbody.

376 *Mottled Mudstones (facies Mp)* are ubiquitous across the study area, with colour
377 varying from a dark reddish brown through to light pink and grey and occasional blue
378 and yellow mottling. Normally massive but with variable development of caliche and
379 gypsum nodules. The tops of beds can exhibit root traces.

380 This facies is characteristic of soil development in semi-arid and arid environments.
381 Mottling is likely the result of the remobilisation of Fe/Mn oxides/hydroxides due to
382 oscillations in the water table (Freytet, 1973) resulting in wetting and desiccation
383 (Alonso-Zarza et al., 2012). While caliché formation is the result of carbonate
384 leaching and precipitation within the soil profile (i.e., Wright, 1990; Goudie, 1996).

385 *Planar laminated sandstones (facies Sp)* are coarse-grained to very coarse-grained,
386 grey litharenites. Beds are < 0.5 m thick with sharp bedding contacts and parallel
387 laminations. This facies likely represents deposition within the upper flow regime
388 owing to the coarse-grain size of the deposits coupled with laminations. Evidence
389 for current flow suggests that these sandstones were deposited from a fluvial
390 system.

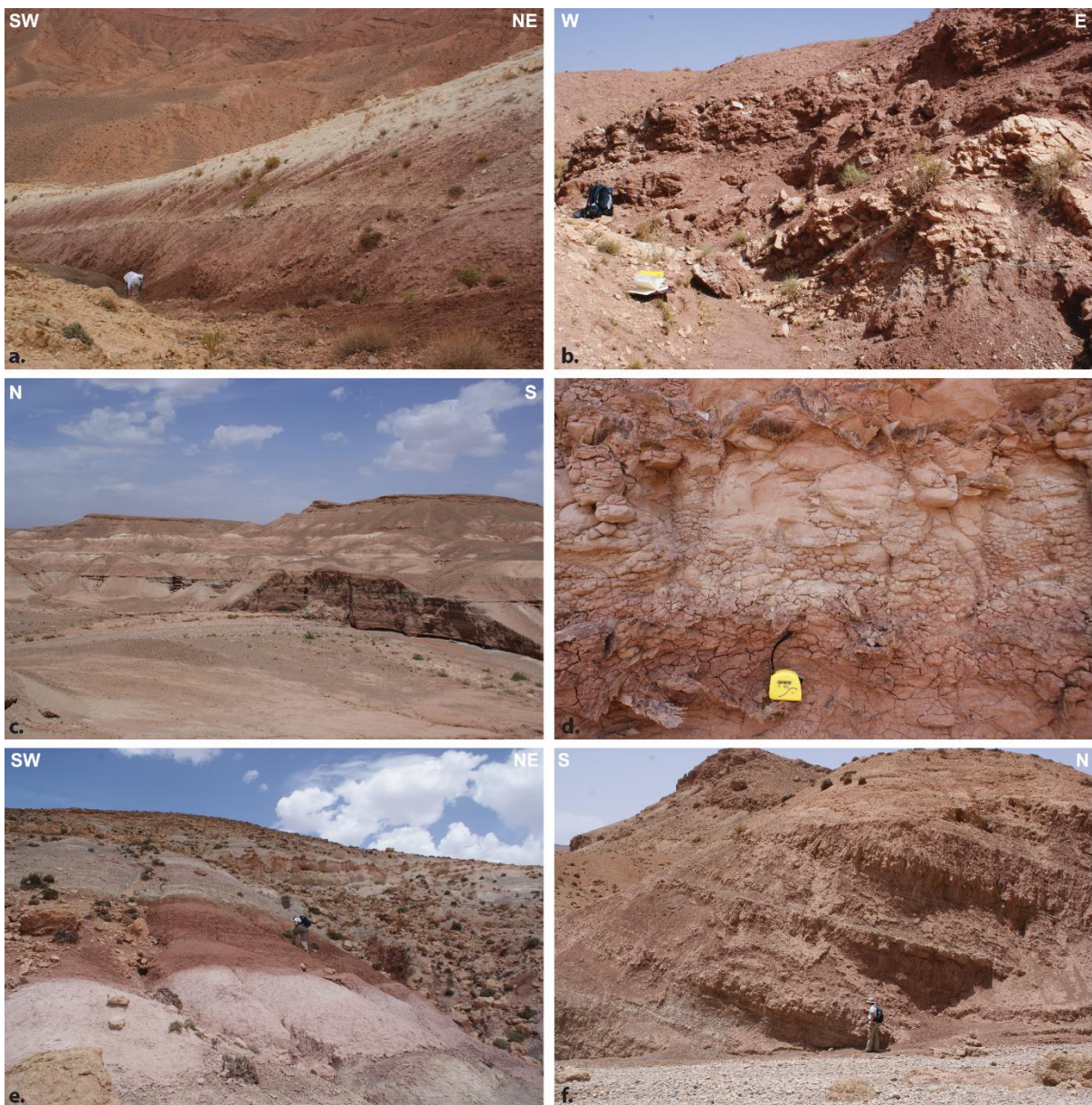
391 *Granular to pebbly sandstones (facies Sch)* facies is composed of sub-rounded to
392 well-rounded, poorly-sorted lithic clasts with a clast-supported texture. The bases of
393 the beds are sharp and often erosional into lower strata, while the beds are laterally
394 discontinuous over 10s of metres. The morphology of these beds is highly
395 suggestive of fluvial channels with a later sediment fill, possibly of small bar forms
396 but no clear sedimentary structures were observed in the field.

397 *Clast-supported conglomerates (facies Gc)* are composed of sub-angular to sub-
398 rounded, poorly-sorted lithic clasts with a clast-supported texture. Beds are massive
399 with sharp bases and variable erosion into underlying sediments. This facies is
400 characteristic of sheet floods, and could represent distal alluvial fan deposition.

401 *Fibrous gypsum (Gf)*, beef or satin spar is composed of needle shaped crystals
402 forming bedding parallel sheets up to a few centimetres in thickness, with the
403 crystals orientated perpendicular to the bedding planes. This gypsum form is
404 common in mudstone facies. This type of gypsum is a secondary precipitate from

405 meteoric water. Growth of such bedding parallel veins is thought to relate to vein
406 opening probably relating to dehydration of gypsum elsewhere in the basin or the
407 effect of tectonic stress (Cobbold et al., 2013).

408 *Selenite (Gy)* crystals up to 30 cm in length occur as isolated crystals in mudstone
409 facies or forming gypsiferous conglomerate (facies Gg) with gypsum crystals
410 randomly oriented within a lime mudstone matrix. Individual selenite crystals likely
411 formed by upward growth from the sediment water interface in shallow water brine
412 pools. The matrix-supported conglomerate likely represents reworking of such
413 crystals potentially down slope in a debris flow.



414
415 *Figure 6a) Photograph of section 1 showing interbedded red mudstones and carbonates; b) Base of*

416 the section 2 showing first occurrences of carbonates in the Aït Ibrim Member. c) Overview of section
417 4 exposed due to Quaternary river incision, d) close up of matrix supported conglomerate formed of
418 large selenite crystals in a mudstone matrix. e) Base of section 6 showing variation in mudstone
419 colour and f) Palaeosols capped by well-developed caliche horizons in location 5.

420 A *gypsarenite (Sg) facies* has been identified in a single location and is composed of
421 sub-rounded, very fine to fine-grains of detrital gypsum. Bedding is massive. A lack
422 of sedimentary structures makes it difficult to firmly establish depositional process
423 beyond current reworking.

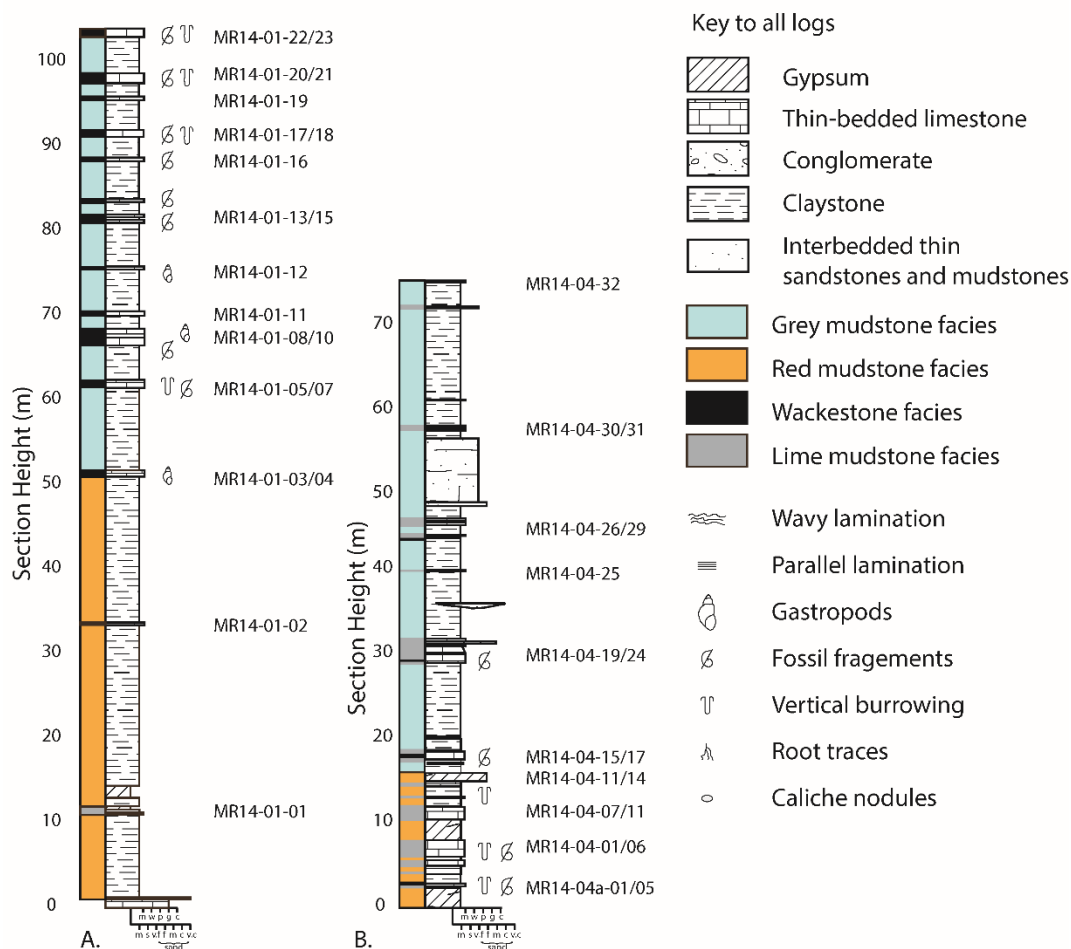
424

425 **Descriptions of studied sections**

426 *Section 1 - Oued Tabia*

427 Section 1 (Fig. 3) is located 5.7 km NE of Toundout, exposed to the north of the road
428 (UTM Zone 29N; 3466678 N 734459 W). The section unconformably overlies
429 Paleogene limestones along a sharp, undulating boundary and is dominated by
430 facies Mp (Figs. 6 & 7a, Table 1) exhibiting various degrees of mottling and
431 palaeosol development, with colour varying from light pink to dark reddish brown. At
432 11 m (Fig. 7a) the sediments become gypsiferous, and small gypsum crystals are
433 present over the next 20 m. By contrast, carbonate beds are rare in the bottom 50
434 m of the section and are generally laterally discontinuous over several metres and
435 lack macrofossil material. However, carbonate becomes more frequent in the upper
436 50 m (Fig. 6a), forming laterally continuous, fossiliferous micrite with pedogenic
437 development (LMF1) and variably intense bioturbation. Gastropods (e.g.,
438 *Melanopsis* sp., *Hydrobia* sp.) are the most conspicuous and unfragmented
439 macrofossils present. The top surface of many of the carbonate beds are rubbly with
440 pseudo-karst development.

441 Towards the top of the section, palaeosol development is less intense and
442 mudstones are not so mottled, indeed uniform grey mudstones and marls are
443 interbedded with the carbonates in some horizons. Mottling reappears in the last 15
444 m, where yellow, red, black mottling is present and effects mudstone and limestone
445 beds. The dominantly fine-grained sediments conformably transition to the overlying
446 conglomeratic unit at ~ 105 m above the basal unconformity.



447

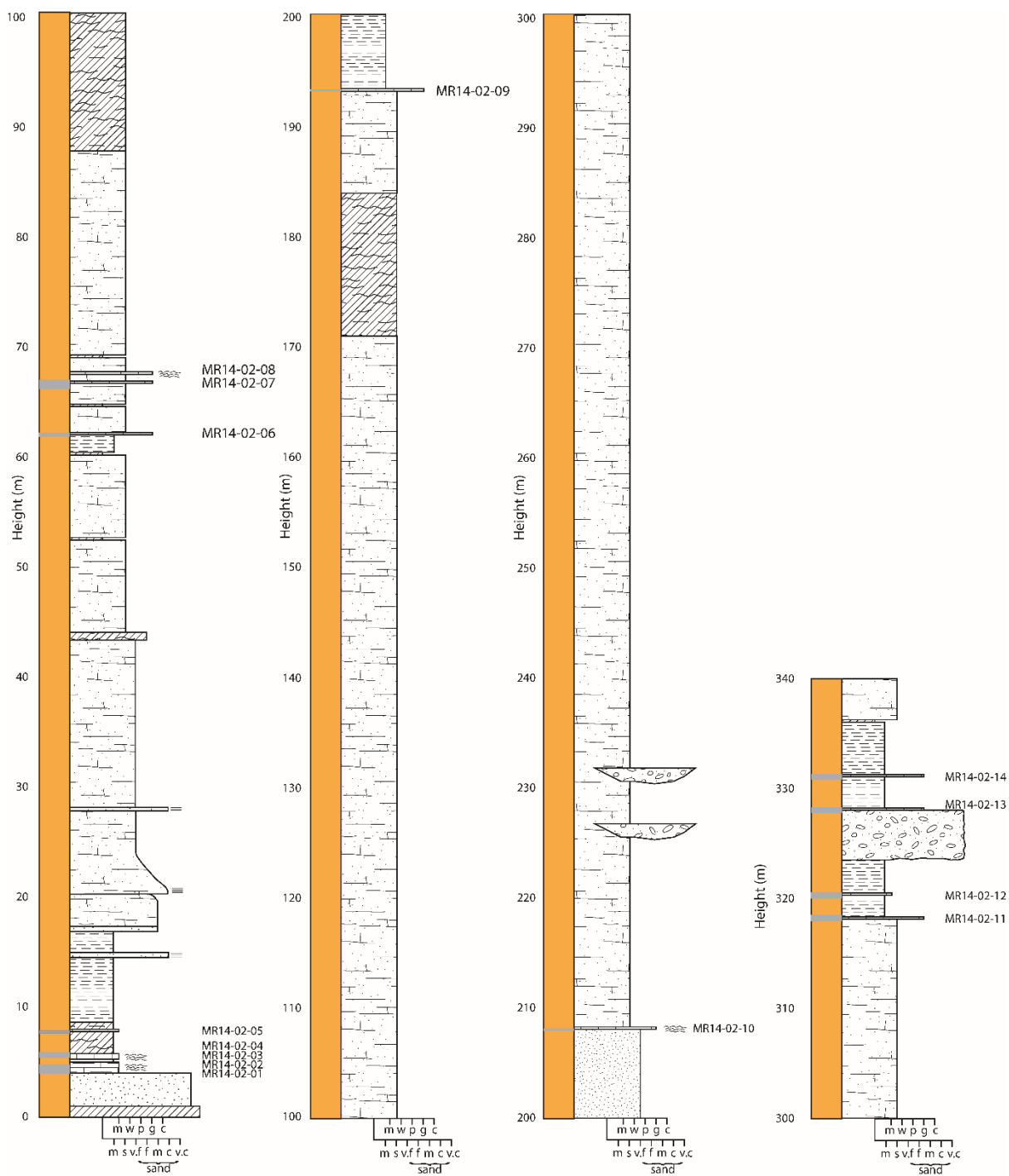
448 *Figure 2 A. Sedimentary log of section 01 measured at Oued Tabia, B. Sedimentary log of the cliff*
 449 *section described from a tributary of the Oued Madri (section 04). Note position of sample numbers*
 450 *used for isotope geochemistry. For the location of the sections see figure 3.*

451

452 **Section 2 – Amekchoud**

453 Section 2 lies ~1.5 km west of Amekchoud (Figs. 3 and 8), exposed in a series of
 454 wadis and associated badland topography, and correlates to part 1 of the
 455 Amekchoud profile sampled by Teson et al. (2010). At the base of the section beds
 456 dip at 55° to the north, gradually decreasing to 35° at the top of the section, the effect
 457 of the syn-sedimentary Amekchoud anticline to the south. The Aït Ibrirn Member
 458 conformably overlies the lower alluvial member (at UTM Zone 29N 3455692 N
 459 727936 W) and is recognised by the first appearance of gypsum with lenses of
 460 interbedded lime mudstone (Fig. 6b).

461 The basal sediments are heterolithic, with thin, 1 – 10 cm thick lime mudstone beds
462 with equally thin red mudstone and fibrous gypsum beds (Fig. 8). Lime mudstones
463 (LMF 1) exhibit well developed wavy lamination and fenestral porosity while the
464 mudstones are massive. Upwards the section becomes dominated by thick, red
465 mudstones, siltstones and muddy fine-grained litharenites. Occasional coarse-
466 grained sandstone beds, 0.3 – 0.5 m in thickness, with planar lamination sometimes
467 form individual horizons or the bases of fining-upwards packages, and thin carbonate
468 and gypsum horizons continue to be present. The middle of the section is
469 dominated by mudstone, gypsum and gypsiferous sandstone, including a 7 m thick,
470 pure white sandstone formed of very fine grains of gypsum, capped by thin,
471 laminated lime mudstones and wackestones (LMF5). At 318 – 338 m, the section
472 again becomes more heterolithic with grey mudstones interbedded between
473 carbonate beds, 0.1 – 0.3 m thick, of LMF5. There is also the appearance of pebbly
474 sandstones and laterally discontinuous conglomerate beds in the upper part of the
475 measured section. Above this interval the unit again returns to red mudstones and
476 sandstones with very minor to no carbonate.



477

478 *Figure 8. Sedimentary log of the Amekchoud section (Figure 3).*

479

480 *Section 4 – Oued Madri tributary*

481 This section lies 3.5 km north of the small village of Aït Said O Mansour (Fig. 3),
 482 along a tributary of the River Madri (UTM Zone 29N 3449413N 725043W). The
 483 section is exposed in cliffs formed by the Quaternary incision of the river (Fig. 6c).

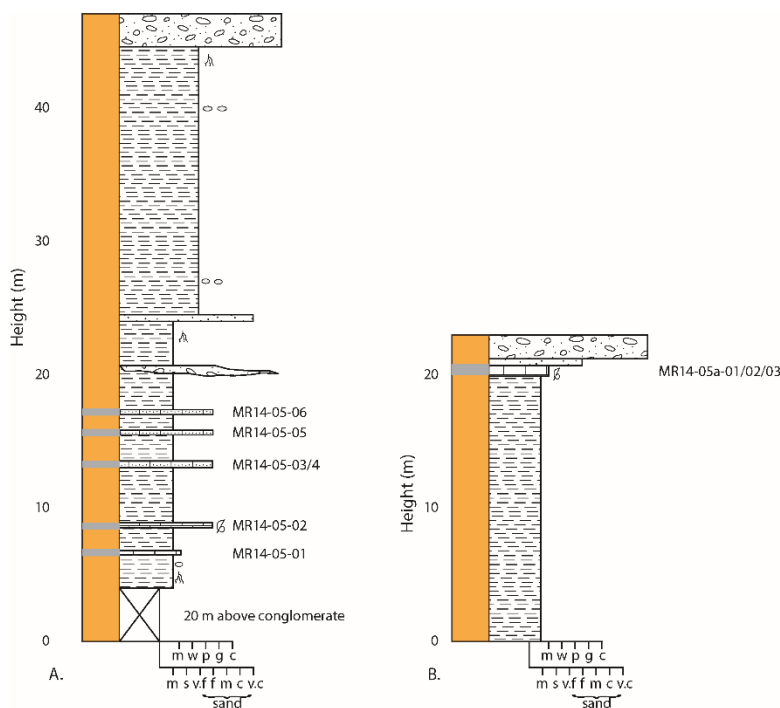
484 Bedding is horizontal, lying on the southern limb of the Amekchoud anticline. The
485 base of the member is not exposed in this location.

486 This section is characterised by much greater numbers of limestone beds than
487 observed in other sections and by the presence of black mudstone horizons (Fig.
488 7b). The lower 20 m of the section is gypsiferous with large selenite crystals present
489 forming discrete horizons. Especially of interest is a 0.6 m thick matrix-supported
490 gypsum breccia, formed of shards of gypsum up to 0.3 m in length in a lime
491 mudstone matrix (Fig. 6d). Elsewhere in the section gypsum is observed as
492 occasional crystals located in the mudstone facies and becomes rarer up section;
493 gypsum is not observed above 20 m in the measured section. Carbonate beds are
494 lime mudstones (LMF1) or charophytic wackestones (LMF7) that exhibit variable
495 amounts of vertical burrowing and often fine upwards from wackestone to mudstone
496 but otherwise are lacking in other primary sedimentary structures. The beds are
497 0.05 – 0.3 m in thickness, but may form amalgamated bed sets of > 1 m thick. Many
498 of the carbonate beds are immediately underlain by thin (c. ≤ 5 cm) horizons of dark
499 grey to black, organic mudstones rich in microfossil material (e.g., ostracods,
500 otoliths). The section consists of four packages of sediment that commence with the
501 organic black mudstones then transition up into limestones followed by red sandy
502 siltstones and mudstones with occasional coarser grained sandstone horizons.

503

504 *Section 05 – Oued Dades Valley, Ait Seddrat Basin*

505 This sequence is represented by a composite section from two localities 2 km apart
506 along strike, it is noticeable that unit thickness is much reduced in this area at ~ 60
507 m. Here the Ait Ibrirn Member overlies only a thin veneer of the lower alluvial unit,
508 which forms the lowermost fill of the Ait Seddrat basin in the Oued Dades valley.
509 This section is dominantly composed of well-developed palaeosols (Figs. 6f & 9) with
510 rare individual beds of poorly developed lime mudstone, although bivalve and
511 gastropod fossil fragments are observable in hand specimen. Calcareous
512 litharenites (carbonate facies 5) cap the top of the well-developed palaeosol
513 sequences. Grainsize increases upwards as cobble conglomerates appear in the
514 section. The upper palaeosol beds are intensely mottled and exhibit well developed
515 root structures and calcrete nodules.



516

517 *Figure 9. Sedimentary log from the Oued Dades region, section A (UTM Zone 29N, 3481286N*
 518 *782241 W) and B (UTM Zone 29N 3481002 N 781221 W) are located ~ 2 km apart along strike. The*
 519 *top conglomerate in section A was traced along strike and section B was measured above this*
 520 *horizon.*

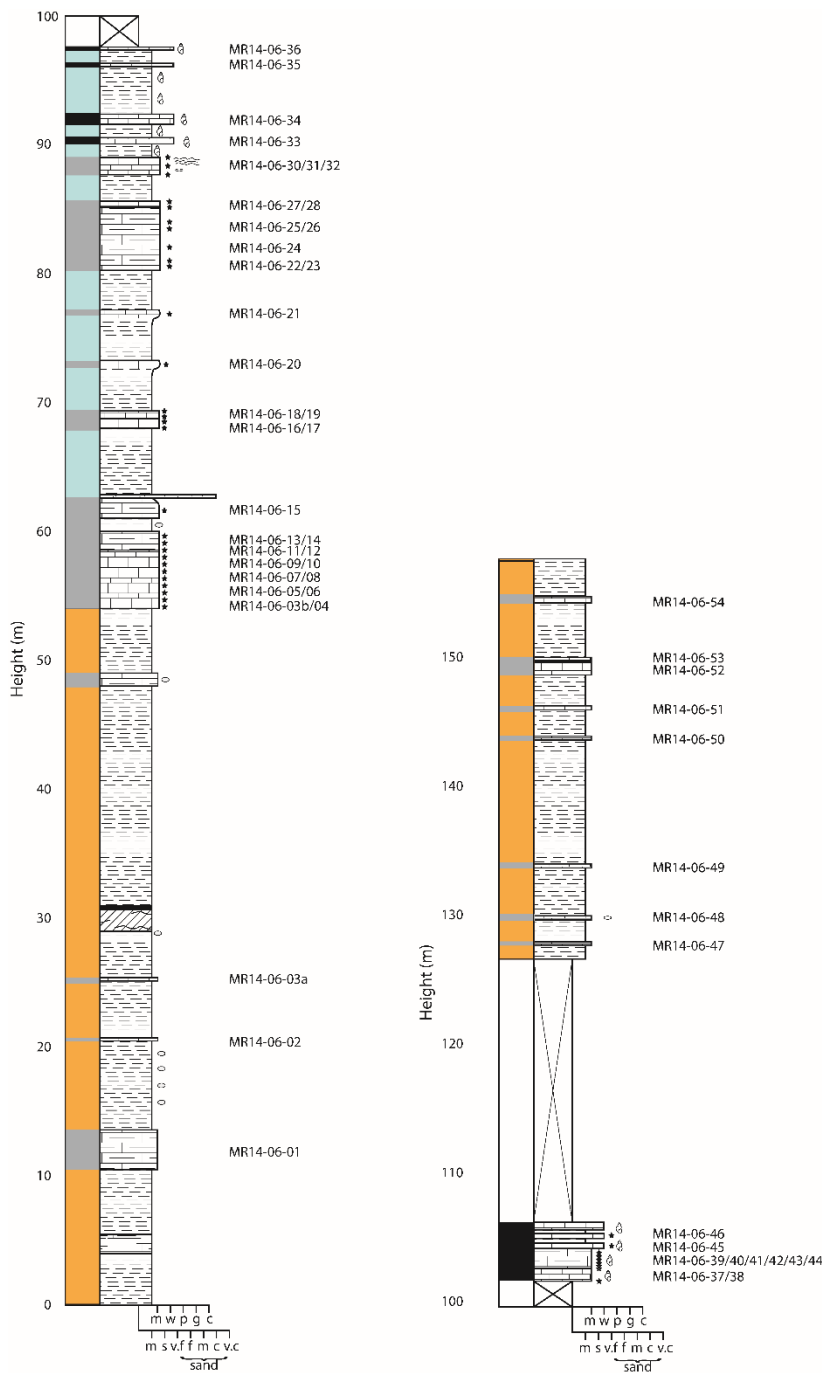
521

522 *Section 06 – Afoud*

523 The Afoud section was measured by Banammi et al. (1996), although their exact
 524 transect could not be established in the field we are confident that the section
 525 measured here (Fig. 3) is close to their AF7 location. This section is in the centre of
 526 the Aït Kandoula Basin (UTM Zone 29 N 3458548N 772547W).

527 The basal part of the section is composed of variably developed palaeosols capped
 528 by well-developed calcrete horizons (Figs. 6E & 10). At 55 m, thick beds of marly
 529 limestone and lime mudstone (LMF1) appear. These beds are nodular, have marly
 530 partings and often have rubbly tops. Limestone beds are interbedded mainly with
 531 grey mudstone and become thicker and coarser-grained up sequence (LMF1 and
 532 LFM8). Spar-filled voids (birds eye fenestrae) are common in the thicker beds. One
 533 1.5 m thick bed is capped by 0.25 m of algal laminations. This 25 m part of the
 534 sequence is rich in gastropods, which are found in both the carbonate and
 535 interbedded grey mudstone beds. The upper part of the member returns to a red
 536 mudstone dominated sequence with isolated wackestone beds that occasionally

537 contain birds-eye fenestrae before transitioning into conglomerates and sandstones
 538 of the overlying alluvial member.



539
 540 *Figure 10. Sedimentary log of the Afoud section (06) in the Ait Kandoula Basin. Location of*
 541 *the section shown in figure 2.*

542
 543 **Facies Associations**

544 *Marginal, evaporative facies associations*

545 The dominance of mottled mudstone facies characteristic of palaeosol development
546 with thin lime mudstones and presence of gypsum suggests that sections 2
547 (Amekchoud), 5 (Oued Dades) and the base of sections 1 (Oued Tabia) and 6
548 (Afoud), predominantly represent alluvial plain settings with periodic influence of
549 marginal lacustrine environments represented by the thin terrestrial carbonate
550 horizons (Fig. 11). The abundance of subaerial features, root traces, mottling, etc.,
551 indicates that the wetlands were subjected to frequent emergence and pedogenic
552 alteration. The mottling is indicative of water table fluctuations resulting in the
553 migration of iron, manganese and calcium due to changes in the reduction potential
554 of the sediment (Freytet and Verrecchia, 2002). High rates of evaporation and the
555 presence of high-salinity water are also indicated by the presence of gypsum both as
556 primary and reworked facies. The rare coarse-grained sandstones and channelised
557 conglomerates observed at Amekchoud (section 2) may represent occasional
558 deposition from active stream channels crossing the mudflats/plains. Furthermore,
559 the carbonate beds are generally laterally continuous with little erosion evident in the
560 sequence and are representative of shoreline deposition (Fig. 11a). This facies
561 association is characteristic of the '*Evaporitive*' lacustrine association of Carroll and
562 Bohacs (1999) and Bohacs et al. (2000) and represents shallow water lake margin
563 sedimentation.

564

565 *Deeper water carbonate lake facies association*

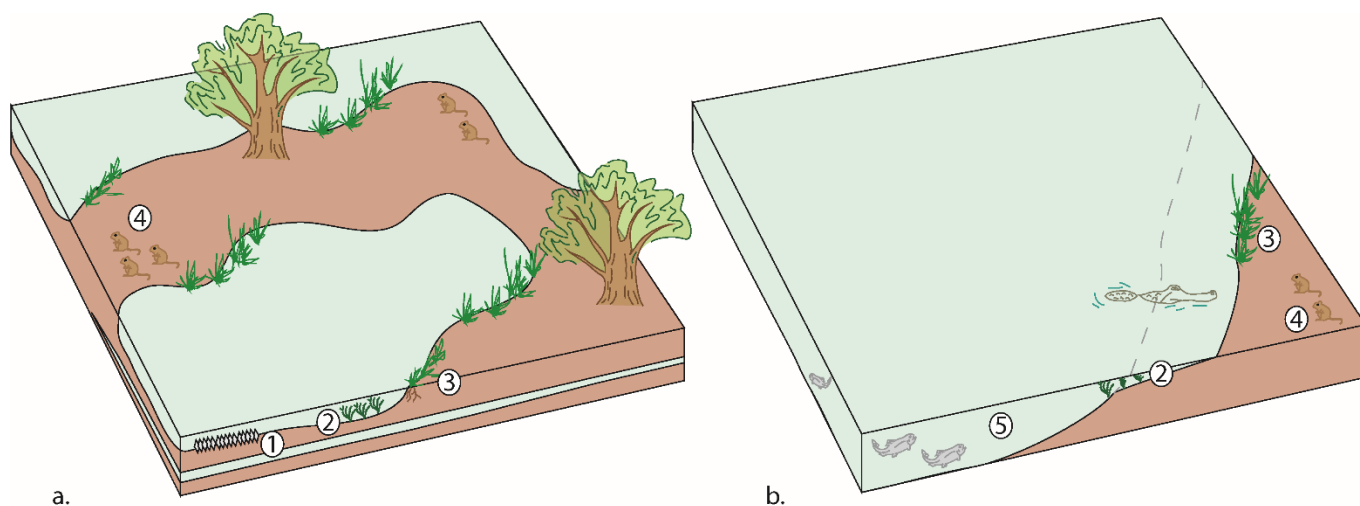
566 The sedimentology of the Oued Madri (Section 4) and upper Afoud (Section 6)
567 sections still show abundant evidence of pedogenic modification, yet the limestone
568 facies in these sections are thicker and more developed than observed in the
569 marginal lacustrine facies associations. Charophyte material is abundant and
570 suggests that the photic zone was relatively free of sediment (Dunagan and Turner,
571 2004), supported by the low amount of detrital quartz observed in thin section.
572 Abundant bioclastic material and burrowing suggests also that the water bodies were
573 normally oxygenated. Although the presence of evaporites in lower part of the Oued
574 Madri section indicates that at times evaporation would have been high likely leading
575 to salinity variations, also previously suggested by Görler et al. (1988). In addition,
576 the presence of glaebule and intergranular cracking observed in thin section

577 indicates that limestones were still affected by later pedogenesis and subaerial
578 exposure (palustrine conditions).

579 The Oued Madri section in particular is interesting as there are defined sequences of
580 organic rich mudstone, limestone, followed by mudstone plus or minus sandstones.
581 These are interpreted as transgressive systems tracts (TST) and highstand
582 sequences as described by Bohacs et al. (2000). Where the thin clastic beds are
583 interpreted as sheet flows representing the rejuvenation of fluvial systems during
584 the TST. These deposits are overlain by typical lake sediments, commonly enriched
585 in organic material, recording the rapid inundation of a low relief surface. Peak
586 organic enrichment has been recognised in many evaporative lake systems just
587 above the TST probably the result of an increase in primary productivity (i.e., Wilkins
588 Peak Mb., Green River Formation., Bohacs, 1998), represented in this section by the
589 thin black mudstone horizons. Overlying carbonate mudstones and wackestones
590 represent deposition from suspension or reworking of material from the littoral zone
591 during the maximum lake extent.

592 Therefore, these sections represent areas in the basin where more persistent lakes
593 developed in the Tortonian (Fig. 11b), as indicated by facies associations and bed
594 thicknesses. The marls likely represent the periods of more persistent and deeper
595 water lacustrine conditions, while limestone beds reflect shallower water deposition.
596 The presence of pedogenic features indicates that even in these areas desiccation
597 and pedogenic alteration was common during lowstands.

598



599

600 *Figure 11. Conceptual models for the a) shallow water marginal environment and b) deeper*
601 *water lacustrine facies associations of the Ouarzazate Basin; 1) mudstones with gypsum, 2)*
602 *various wackestones, 3) pedogenic overprinting; 4) palaeosols (with a range of*
603 *micromammal fossils e.g., Benammi et al., 2005; 2006) and 5) grey and black mudstones*
604 *and lime mudstones with ostracod, bivalve and fish fossils.*

605

606 **Stable Isotopes**

607 Alteration of primary depositional and pedogenic phases can be determined through
608 petrographic and cathodoluminescence microscopy. Non-luminescent cements and
609 an abundance of vadose and subaerial exposure features are suggestive of
610 carbonates that have undergone early diagenesis (Valero-Garcés and Aguilar,
611 1992). Analysis of samples shows mainly dull to moderate luminescence of the
612 micrite with most variability related to glaebule formation (Fig. 5). Combined with a
613 range of features related to subaerial exposure, suggests that these sediments
614 underwent early diagenetic stabilisation and variable post depositional alteration
615 related to palustrine evolution.

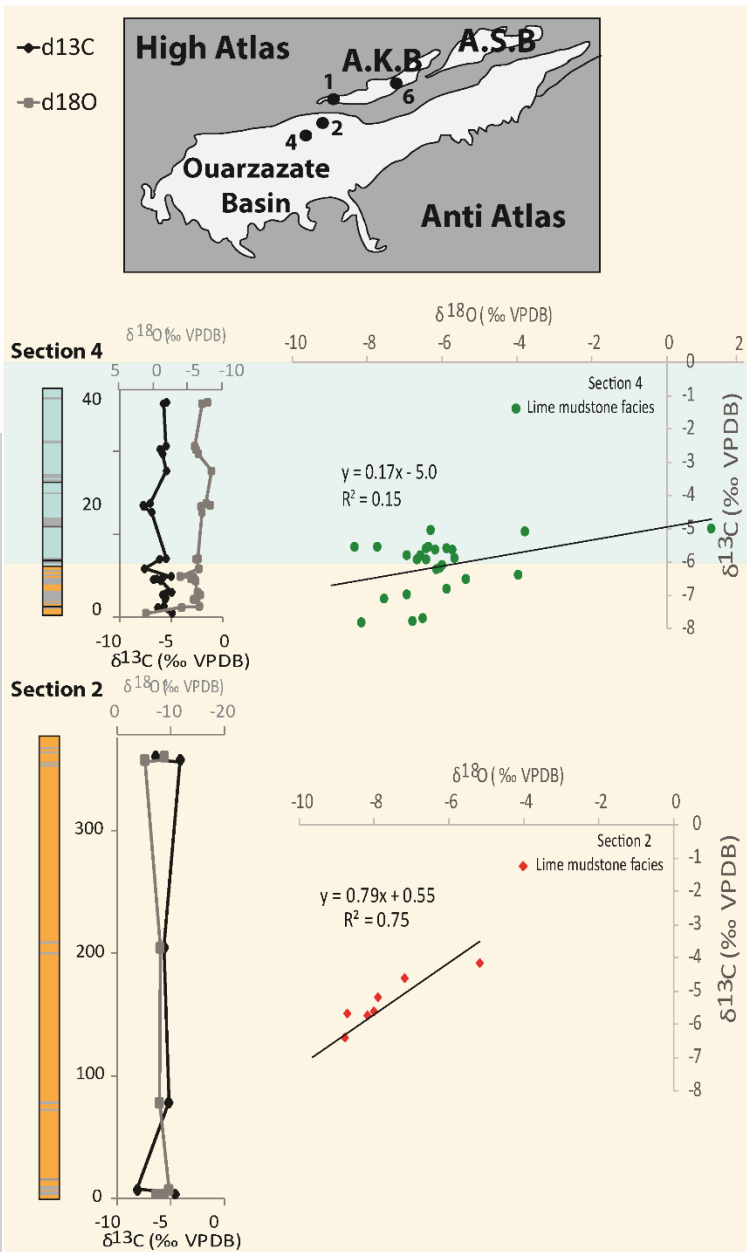
616 Therefore, 120 bulk samples were drilled for stable isotope analysis from areas of
617 micrite away from obvious areas of palustrine alteration. Lacustrine carbonates
618 typically have depleted ratios of $\delta^{18}\text{O}$ and $\delta^{13}\text{C}$ when compared to marine
619 carbonates (Keith and Weber, 1964), and the limestones of the Ait Ibrirn Member are
620 no exception (Fig. 12).

621 Both sections 1 and 4 (Fig. 12) exhibit relatively constant isotope ratios, with no
622 stratigraphically coherent shifts in either $\delta^{13}\text{C}$ or $\delta^{18}\text{O}$ (Fig. 12, Table 2). Carbon
623 isotope ratios are similar in both sections ($-6.0 \pm 1.0\text{‰}$ VPDB), while the average
624 $\delta^{18}\text{O}$ ratio is slightly lower in section 1 ($-8.1 \pm 0.5\text{‰}$ VPDB) than section 4 ($-6.3 \pm$
625 1.1‰). Section 6 is somewhat more variable; a $\sim 3\text{‰}$ negative shift in both $\delta^{13}\text{C}$ and
626 $\delta^{18}\text{O}$ occurs over a 40 m interval in the middle of the section. The most negative
627 values are associated with the deeper water lacustrine facies association. The
628 overall isotope values ($\delta^{13}\text{C} = -5.6 \pm 1.1\text{‰}$; $\delta^{18}\text{O} = -5.8 \pm 2.1\text{‰}$) are like those in
629 sections 1 and 4. Sections 2 and 5 also exhibit similar overall isotope values.

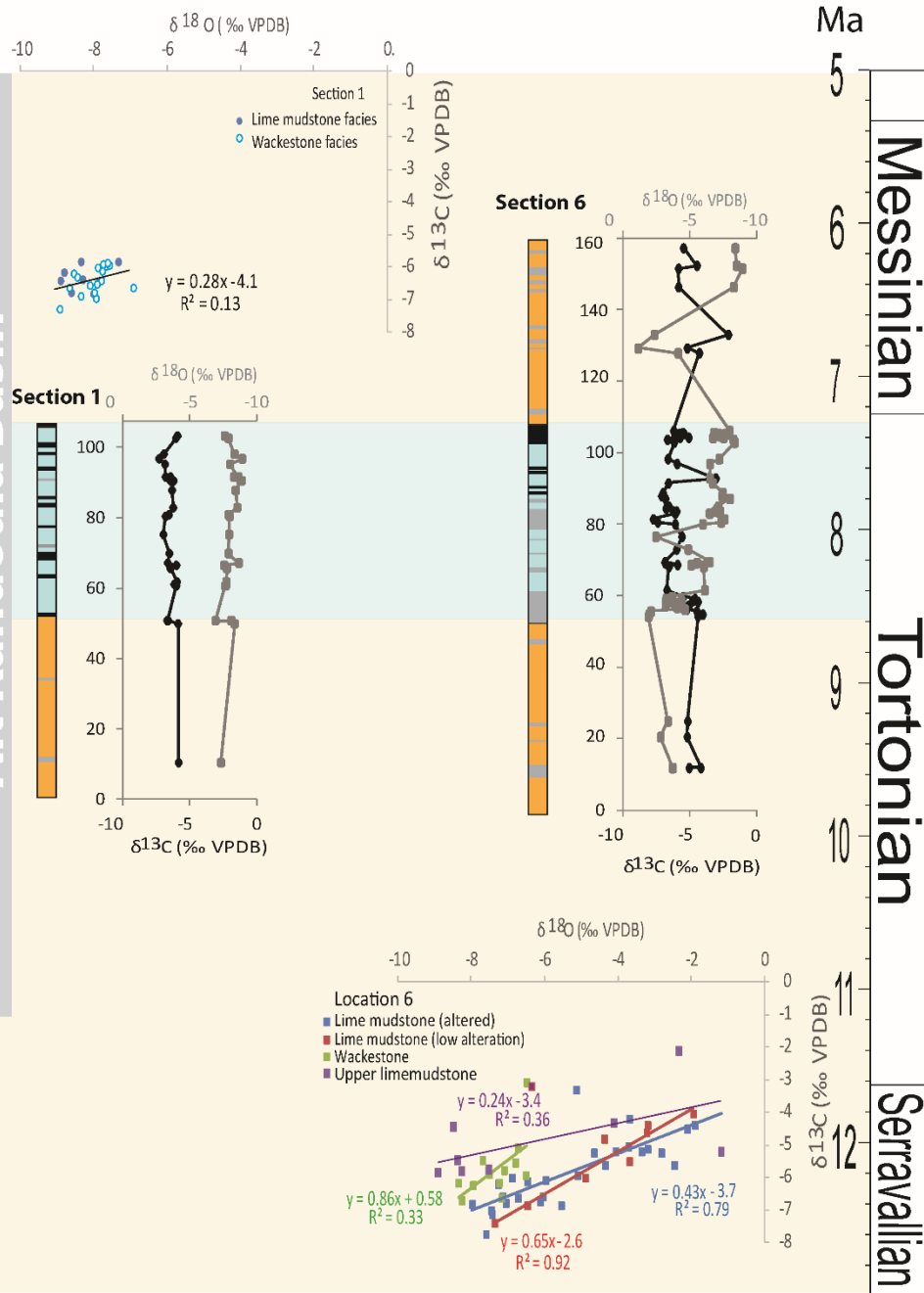
630 The isotopic composition of samples has also been considered by carbonate facies
631 type at each location (Fig. 12), as not all samples were thin-sectioned this has been
632 simplified into either lime mudstone or wackestone facies recognisable in hand
633 specimen. In addition, the amount of palustrine alteration has been qualitatively
634 assessed as either being low (no or negligible visible alteration) or present (obvious
635 visible alteration in the hand specimen). Most specimens show some evidence for
636 palustrine alteration apart from in section 6 samples where little obvious alteration is
637 present in some samples.

638 *Figure 12 (next page). Stable isotope compositions of the micrite from sections 1 to 4*
639 *studied plotted by section height showing the vertical change in isotopic composition through*
640 *the sections combined with isotope cross-plots for each section, facies association is*
641 *indicated by colour where orange represents shallow water and blue represents deep water*
642 *facies. Key to logs is shown on figure 7. Also included is a location map showing location of*
643 *the Ouarzazate and Ait Kandoula Basins and approximate geological timescale. Isotope*
644 *results are reported in standard delta-per-mil (‰) relative to PDB.*

Ouarzazate Basin



Ait Kandoula Basin



646

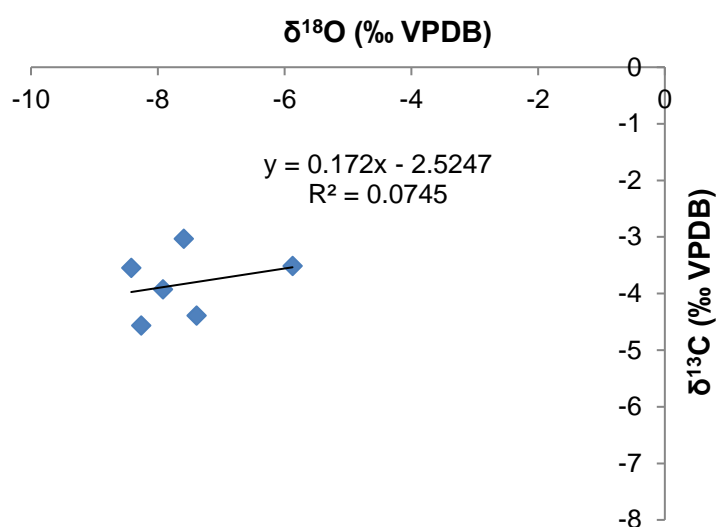
647 Section 2 is the oldest section dating to ~12.5 – 10 Ma (Teson et al., 2010) with
648 facies dominated by lime mudstone. These isotopic data plot in a single domain and
649 have a clear covariant trend with an r^2 of 0.75, and the regression line has a gradient
650 of 0.79 (Fig. 12).

651 Sections 4 and 6 date to ~ 10 – 7 and 9 – 6 Ma, respectively (Benammi et al., 1995;
652 1996; Benammi and Jaeger, 2001). These sections have the most extensive
653 carbonate records and have more variable isotope ratios than the other sections
654 sampled. Section 4, dominated by lime mudstone, exhibits variable $\delta^{18}\text{O}$, while $\delta^{13}\text{C}$
655 is somewhat less variable. Overall, the $\delta^{13}\text{C}$ and $\delta^{18}\text{O}$ show a weak co-variant trend
656 with an r^2 value of 0.15 (Fig. 12).

657 Section 6 has the greatest sample density across wackestones, and low to clearly
658 altered lime mudstones. When all data are plotted together there is a clear covariant
659 trend with an $r^2 = 0.35$. However, when facies are plotted separately, the mudstone
660 and wackestone facies do not plot in the same isotopic domain (Fig. 12). The
661 wackestones have lower $\delta^{18}\text{O}$ of -6.5 to -8.5 ‰ in comparison to the majority of the
662 lime mudstones that have $\delta^{18}\text{O}$ as high as -1 ‰, although $\delta^{13}\text{C}$ values are
663 comparable across all samples. Furthermore, the covariant trend is steeper and has
664 an r^2 of 0.33 for the wackestones, although the origin of the covariant trend appears
665 consistent with the mudstones in the lower part of the section. The lime mudstone
666 facies can be split further into low and present palustrine alteration, and between the
667 lower (below 55 m) and upper (above 120 m) parts of the section. Below 55 m lime
668 mudstones with little and clear alteration have been analysed, both populations of
669 data sit in the same domain and show a clear covariant trend; however, the r^2 values
670 of the two data sets is different with the clearly altered sediments having an r^2 of 0.79
671 and the low alteration set a r^2 of 0.92. This observation is an indication that
672 palustrine alteration increases the scatter on the $\delta^{13}\text{C}$ values in particular, similar
673 observations have been made in the Miocene lacustrine systems of Spain that were
674 also subjected to post-depositional pedogenesis (Arenas et al., 1997; Alonso-Zarza
675 et al., 2012). By contrast, fewer carbonate beds are present above 120 m but these
676 plot in a similar domain to the wackestones and the regression line has an r^2 value of

677 0.36. Of note is that the slope of the line (0.26) is lower than for all the regressions
678 on data lower in the sequence.

679 Sections 1 and 5 are the youngest studied intervals, and are thought to date to ~ 9 -
680 5 Ma (Benammi et al., 1996), although the age of section 5 is poorly constrained.
681 Section 1 is dominated by gastropod-bearing wackestone with fewer lime mudstones
682 than in the other sections; however, both facies plot in the same isotopic domain.
683 When the two variables are cross-plotted, there is a weak covariant trend with an r^2
684 of 0.13 when all isotope data for this location are taken into account (Fig. 12). By
685 contrast, the isotopic analysis from section 5 shows little variance in either $\delta^{18}\text{O}$ or
686 $\delta^{13}\text{C}$ with an r^2 of 0.07 (Fig. 13). In addition, the data plot in a different isotope
687 domain with lower $\delta^{13}\text{C}$ (< 4.5 ‰) than the other samples tested, although the slope
688 of the regression line is 0.17 and therefore similar to sections 1, 4 and the upper part
689 of section 6.



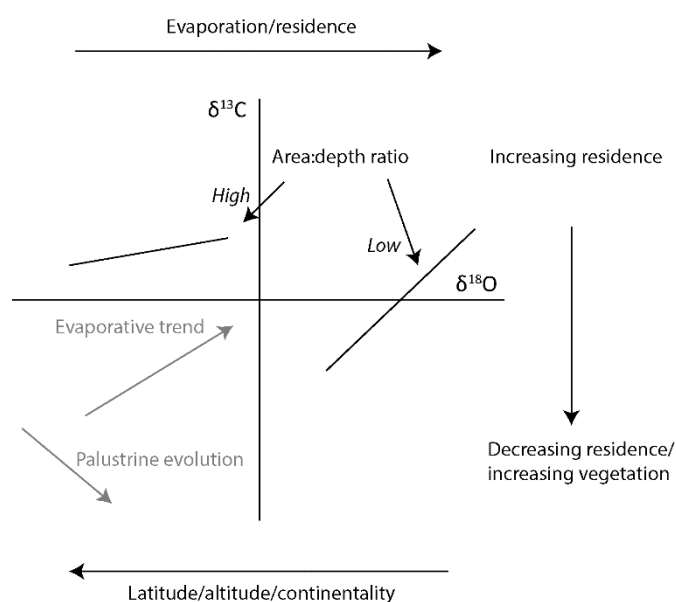
690

691 *Figure 13. $\delta^{18}\text{O}$ / $\delta^{13}\text{C}$ cross-plot of section 5.*

692

693 Discussion

694 *Implications of isotopic variations laterally and vertically*



695

696 *Figure 3. Summary of principal environmental controls on oxygen and carbon covariant*
 697 *trends in lacustrine sediments (modified after Talbot, 1990; Arenas et al., 1997). Increasing*
 698 *evaporation or residence time results in more positive $\delta^{18}\text{O}$ values, whereas increasing*
 699 *latitude, altitude or continentality results in more negative $\delta^{18}\text{O}$ values. By contrast, $\delta^{13}\text{C}$*
 700 *values become more positive in dry catchments and more negative in humid/well vegetated*
 701 *catchments. Post-depositional palustrine alteration of sediments will also move $\delta^{13}\text{C}$*
 702 *towards more negative values.*

703

704 Section 2 is the oldest section studied (~12.5 – 10 Ma; Teson et al., 2010), and is
 705 located in the main Ouarzazate Basin. The covariant trend with an r^2 of 0.75 (Fig.
 706 12) is strong evidence that these carbonates were deposited in a hydrologically
 707 closed lake, as it has previously been demonstrated that strong positive correlations
 708 ($r^2 > 0.7$) are characteristic of carbonate precipitation in closed lake environments
 709 (Talbot, 1990; Talbot and Kelts, 1990). This interpretation is supported by the
 710 presence of evaporites typical of such environments. Stratigraphically higher,
 711 section 4, represents the evolution of the Ouarzazate Basin lacustrine system.
 712 Although there is still a weak covariant trend the r^2 (= 0.15) indicates a hydrologically
 713 open lake (Talbot, 1990). Yet a positive $\delta^{18}\text{O}$ value indicates that there was either
 714 intense evaporation at the base of the section or that residence times were relatively
 715 long (Fig. 14), as hydrologically open lakes typically have only small variations in
 716 $\delta^{18}\text{O}$ (Talbot, 1990). It is also possible that these basal sediments may still be
 717 recording a closed lake signal that progressively becomes more open up section, or
 718 that later pedogenesis has resulted in a loss of primary carbonate signatures
 719 resulting in lighter carbon values (Alonso-Zarza et al., 2012). Plant respiration

720 promotes enrichment in ^{12}C in the substrate that can obscure the original isotopic
721 trend (Dunagan and Driese, 1999; Tanner, 2000), yet Alonso-Zarza et al. (2012)
722 demonstrated the pedogenesis does not completely obscure the original lacustrine
723 isotopic signature. This conclusion is also supported by the data from section 6
724 studied here, where increased pedogenic alteration increases the data variability but
725 does not obscure original trends. Therefore, we interpret that the Ouarzazate Basin
726 lacustrine system evolved from a closed basin in the Serravalian to an open system
727 in the Tortonian.

728 Interestingly, there is also a decrease in steepness of the regression line from $s =$
729 0.79 to $s = 0.17$ from section 2 to section 4, suggesting that the area/depth ratio of
730 the lacustrine system had shifted (Fig. 14). It is unlikely that the lake became
731 shallower over time given the sedimentary evidence of deeper water facies, instead
732 we favour the interpretation that the area of the lakes became much greater at this
733 time (Talbot, 1990). The origin of the covariant trends from the two sections is similar
734 suggesting that the original isotopic compositions of the water masses feeding the
735 lacustrine system was unaltered.

736 Section 6 is the same age as section 4 but located in the Aït Kandoula thrust top
737 basin. There are sub-parallel trends between the isotopic value of the wackestones
738 and lime mudstones, the slope of the two regression lines is 0.86 and 0.65 ,
739 respectively. However, the wackestones indicate an open lacustrine system as do
740 the youngest lime mudstones ($r^2 = 0.33$ and 0.36 , respectively). Whereas the older
741 lime mudstones, showing less palustrine alteration, indicate a closed basin ($r^2 =$
742 0.92).

743 In addition, there is a clear stratigraphic trend up section in both $\delta^{18}\text{O}$ and $\delta^{13}\text{C}$ (Fig.
744 12). At the 55 m level, where limestone beds become thicker and more common,
745 values of $\delta^{18}\text{O}$ and $\delta^{13}\text{C}$ are high. The succeeding 50 m of deposition exhibit a
746 coherent drop in $\delta^{18}\text{O}$ and a smaller decrease in $\delta^{13}\text{C}$. Extensive carbonate
747 deposition ends at the 105 m level, with the few overlying thin carbonate beds
748 exhibiting higher and more variable $\delta^{18}\text{O}$. Taken with the physical sedimentology,
749 extensive and thicker carbonates, change in mudstone colour and widespread
750 gastropod shells from ~90 to 105 m, the isotope data suggests that the lake at
751 section 6 was initially an evaporative and salty endorheic basin. The lake then

752 progressively freshened, low r^2 values suggest that the lake became hydrologically
753 open during the middle of the section. Similarly section 1, along strike from section
754 6, has low and stable values of $\delta^{18}\text{O}$ and $\delta^{13}\text{C}$ suggesting that evaporative
755 drawdown was relatively limited at these sites during intervals of carbonate
756 deposition. This suggestion implies that water residency times were short and the
757 poor correlation of the covariance trend indicates that during deposition the
758 lacustrine system was hydrologically open (Talbot, 1990).

759 The age of section 5 is unclear as no age constraints have been published for the Aït
760 Seddrat Basin. Samples for this area are from carbonates with significant pedogenic
761 overprint, although data from elsewhere in the basin and Alonso-Zarza et al. (2012)
762 demonstrate the original trends have been preserved. Therefore, our limited
763 samples suggest deposition in an open lacustrine system and coeval deposition with
764 the top of section 6, suggesting that section 5 is of late Tortonian to Messinian in age
765 based upon existing dating (Benammi et al., 1995;1996). Also of note, is that the
766 isotopes from section 5 sit in a different isotopic domain compared to the other
767 sections. This observation can be explained as section 5 is located in the Aït
768 Seddrat thrust-top basin, to the east of the Aït Kandoula and Ouarzazate basin
769 sediments, indicating the Aït Seddrat Basin was not connected to the rest of the
770 lacustrine basins at this time.

771 These new isotope data show for the first time that the Miocene Ouarzazate lake
772 system evolved from an initial hydrologically closed condition in the Serravallian to
773 early Tortonian into an open lake system in the late Tortonian.

774

775 *Miocene palaeoenvironments*

776 The facies associations identified in the Middle Miocene sediments of the
777 Ouarzazate Basin fall into two groups, one indicating shallow, ephemeral lacustrine
778 conditions typical of the 'evaporative' facies of Carroll and Bohacs (1999) and the
779 other more persistent and deeper water environments (Fig. 11). It is likely that the
780 grey marls and overlying carbonate horizons indicate periods of highest water levels
781 and freshest water in the basin. Combined with the stable isotope evidence, these
782 data suggest that the Aït Ibrirn Member of the Aït Kandoula Formation was deposited

783 in an lacustrine system that was initially hydrologically closed but over time became
784 a hydrologically open system.

785 Initial carbonate deposition started around 12.5 Ma, and is represented by section 2
786 and the base of sections 1, 4 and 6. The palaeolake system was possibly confined
787 to smaller pools prone to evaporite deposition due to the higher salinity of the waters,
788 with carbonate deposition taking place during highstands (Fig. 11a and 15). These
789 were surrounded by a playa of mudflats and marshes, where soil development
790 overprinted older sediments resulting in the widespread palustrine facies observed
791 especially during lake level lowstands (Fig. 11a). These type of palustrine systems
792 with fluctuating water levels have been described elsewhere in the Mediterranean
793 during the Miocene (i.e., in Turkey; Alciçek & Alciçek, 2014, and in Spain; Arenas
794 and Pardo, 1999; Saez et al., 2007). Even though, lake levels were low there
795 appears to have been limited transport of coarse alluvium into the basin in the areas
796 studied, suggesting that alluvial material was mainly being trapped in mountain front
797 alluvial fans and that only sandy bedload and muddy suspended load was
798 transported further out into the basin. Only occasional sheet floods and small
799 channels transported coarse-grained material out into the foreland basin. As the
800 Ouarzazate Basin was hydrologically closed at this time, it is reasonable to assume
801 that high evaporation combined with low water input led to seasonal flow in the river
802 systems and the termination of over ground flow in the remaining pools. These
803 characteristics are typical of an underfilled lake basin (c.f., Carroll and Bohacs, 1999)
804 where accommodation space exceeds sediment flux. As a result lake levels rarely
805 reach sill levels and sediments are dominated by evaporite facies interbedded with
806 alluvial-fluvial strata.

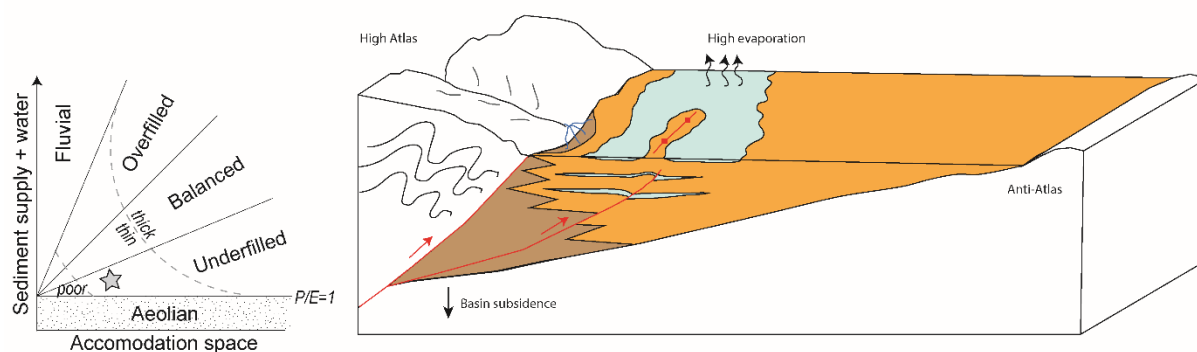
807 During the later Tortonian, it is likely that a lake, covered a large portion of the
808 Ouarzazate Basin (indicated by El Harfi et al., 2001) and its sub-basins (Fig 15).
809 $\delta^{13}\text{C}$ and $\delta^{18}\text{O}$ values indicate that at these times the lake waters were variable in
810 terms of oxygen levels and salinity but overall the system was hydrologically open
811 and had transitioned into a 'balanced-fill' lacustrine system (Carroll and Bohacs,
812 1999). In balanced-fill lakes, accommodation approximately equals sediment supply
813 and periodically surface outflows are developed.

814 Similarities in isotope measurements also suggest that the Ouarzazate and Aït
 815 Kandoula basins were connected. These persistent lacustrine systems resulted in
 816 thick carbonate beds and organic-rich mudstones rich in flora and fauna, interbedded
 817 with thicker sequences of massive, light grey mudstone and siltstone in the main
 818 depo-centres of the basin. The Oued Madri section exhibits five parasequences,
 819 each reflecting lake-level rise and subsequent fall, over ~ 50 m. These short term
 820 variations in lake level, and the changes observed across the wider basin between
 821 high and lowstands in lake level, are likely to be the result of changing
 822 water/sediment supplies determined by climate superimposed on tectonic
 823 subsidence creating the accommodation space in the basin.

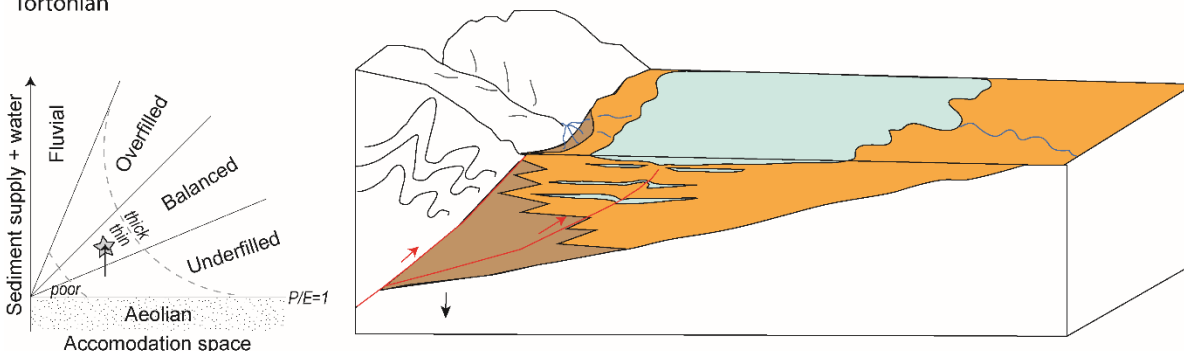
824 The youngest sediments (uppermost section 6 and section 5) indicate that
 825 hydrological open conditions persisted into the Messinian, although by that time the
 826 Aït Seddrat Basin at least was being fed by waters with a different isotopic signature.

827

Late Serravalian to early Tortonian



Tortonian



828

829 *Figure 15. Palaeoenvironmental reconstructions for the Late Serravalian to early Tortonian*
 830 *showing underfilled basin conditions and the Tortonian with deeper and widespread*
 831 *lacustrine facies typical of a open lake. Inset graphs shows Carroll and Bohacs (1999)*

832 *concept for lacustrine deposition with the approximate position of the lacustrine system at*
833 *each time indicated by a star. Reducing accommodation space only, will not result in a*
834 *change from underfilled to balanced filled lakes of any significant thickness; however,*
835 *increasing sediment supply and water will result in this change.*

836

837 *Climatic and tectonic influences*

838 Traditionally continental carbonates are thought to form when there is *relative*
839 tectonic quiescence and when climate was neither too arid, nor too humid to prevent
840 limestone formation (i.e., Cecil, 1990; Alonso-Zarza, 2003; Valero-Garcés et al.,
841 2008; Pla-Pueyo et al., 2009; Valdeolmillos-Rodríguez et al., 2011; Cabaleri and
842 Benavente, 2013; Ashley et al., 2014; de Wet et al., 2015). By contrast, the creation
843 of tectonically induced relief has often been recognised in the rock record by the
844 appearance of conglomerates (e.g., Heller et al., 1988; Flemings and Jordan, 1990;
845 DeCelles et al., 1991; Carrapa and DeCelles, 2008). These ideas led El Harfi et al.
846 (2001) to propose that the conglomerates preceding and following the lacustrine Aït
847 Ibrirn Member were the result of pulses of surface uplift in the High Atlas shedding
848 material into the Ouarzazate foreland Basin. It then follows that the intervening
849 period of lacustrine deposition represents a period of tectonic quiescence in the
850 building of the topography of the High Atlas Mountains (El Harfi et al., 2001).

851 However, other authors propose that tectonic activity in the High Atlas was
852 continuous throughout the Miocene based upon structural relationships (i.e., Teson
853 and Teixell, 2008) and fission track evidence of exhumation (i.e., Balestrieri et al.,
854 2009) (Fig. 2). Indeed, the presence of underfilled (accommodation space >
855 sediment supply) lacustrine deposits suggest high subsidence rates (Bohacs, 1999)
856 incompatible with a model of total tectonic quiescence. High subsidence rates and
857 tectonic activity have been shown to be essential for the formation of other lacustrine
858 systems. For example, the deposition of the lacustrine Green River Formation
859 (GRF) of North America is associated with periods of tectonism in the Eocene
860 (Roehler, 1993; Pietras et al., 2003; Smith et al., 2015), not periods of inactivity.

861 Furthermore, facies models of non-marine foreland basins (e.g., Heller et al., 1988;
862 Flemings and Jordan, 1990; Marr et al., 2000; Clevis et al., 2003; Densmore et al.,

863 2007; Armitage et al., 2011; Allen et al., 2013) demonstrate facies retrogradation
864 should occur when subsidence rates are high as a result of the increased
865 lithospheric loading resulting from thrust emplacement. By contrast, phases of
866 tectonic quiescence and erosional unloading result in the progradation of the gravel
867 facies across the basin and the displacement of longitudinal rivers distally away from
868 the thrust front (Burbank, 1992; Burbank and Vergé, 1994).

869 If this is the case then a Late Miocene to Pliocene slowdown in thrusting would
870 explain the subsequent transition from the lacustrine sediments to the alluvial fan to
871 the Plio-Quaternary conglomerates. A cessation of thrusting in this period has
872 previously been suggested (i.e., Faissinet et al., 1988; Balestrieri et al., 2009) prior to
873 another phase of uplift in the Quaternary (Görler et al., 1998; El Harfi et al., 2001;
874 2006), associated with geomorphic evidence of landscape rejuvenation and gorge
875 formation (i.e., Stokes et al., 2008, Boulton et al., 2014). Although, recent dating of
876 fluvial terraces questions high rates of Quaternary uplift as incision rates are < 0.2
877 mmyr^{-1} over the last ~ 100 ka (Stokes et al., 2018).

878 The lacustrine sediments also record a change from closed to open basins through
879 the Miocene despite an overall increase in apparent water depth. This change in
880 hydrodynamic conditions is likely the result of the breaching of a basin sill in the Late
881 Tortonian due to the filling of available accommodation space and overtopping of the
882 basin or owing to the capture of the basin by another drainage system.

883 Climatic forcing could drive the change from an underfilled to balanced fill system if
884 accommodation space was constant, or increasing, and where sediment/water
885 supply was also increasing (Fig. 13a). The presence of more persistent lakes
886 argues for more water into the basin, potentially due the change from a semi-arid to
887 subhumid climate supporting this argument. Higher lake levels could then have
888 breached a local basin sill.

889 However, the Middle – Late Miocene period is notable for global climatic shifts
890 towards colder and drier climates (Potter and Szatmari, 2009) and in North Africa the
891 Late Miocene is considered at the period when aridification of the Sahara developed
892 (Schuster et al., 2006; Sepulchre et al., 2006). Neither of these trends would
893 account for greater lacustrine activity at this time that would suggest wetter not drier
894 conditions (Fig. 13 inset). Indeed Sepulchre et al. (2006) consider Early to Middle

895 Miocene uplift key for developing the Atlas Mountains as a topographic barrier to
896 moisture, and thus forming the Sahara Desert ~ 8 Ma.

897 A decrease in accommodation space could also result in the filling of the basin and
898 drive the trend in the sedimentary facies to a balanced fill system, despite the
899 sedimentary evidence of more persistent lake facies (Fig. 15). Leprêtre et al. (2015)
900 recently presented evidence for Middle Miocene uplift until ~ 11 Ma, with subsequent
901 cessation of loading. However, a reduction in accommodation space only would
902 result in poor preservation of carbonate facies inconsistent with the sedimentary
903 record. A reduction in subsidence would still need an increase in sediment supply to
904 achieve a balanced-fill lacustrine system with preservation of sediments.

905 Finally, capture of the basin could also drive the observed changes in isotope
906 composition. The Draa River is known to have captured the Dades River, which is
907 the main drainage system of the Ouarzazate Basin, forming a 300 m deep canyon
908 through the Anti-Atlas to the south of the basin. The timing of this event is not well
909 constrained but is generally placed around the Pliocene – Pleistocene boundary, and
910 has been ascribed to both regressive erosion of the Draa and basin overtopping
911 (Stäblein, 1988; Arboleya et al., 2008). Arboleya et al. (2008) reported alluvial
912 deposits of presumed Mio-Pliocene age resting on the crystalline basement of the
913 Anti-Atlas adjacent to the Draa River supporting the overtopping hypothesis for the
914 change from internal to external drainage.

915 Currently the temporal constraints on the sedimentary succession in the Ouarzazate
916 Basin, the timing of thrust events and regional climatic trends are not well enough
917 known to fully unravel the competing controls on basin sedimentation, but it is likely
918 that higher rates of tectonic subsidence led to initial lacustrine deposition within the
919 developing foreland basin. Over time the basin gradually filled up and possibly
920 overtopped a sill, either due to the available accommodation space being exhausted
921 or increased sediment/water supply. Headward erosion of the Draa River, or
922 another palaeodrainage could also have captured the Ouarzazate Basin perhaps
923 driven by periodic basin overtopping. While the ultimate mechanism for the changes
924 between alluvial fan and lacustrine sedimentation and the change in lacustrine
925 hydrodynamic conditions still needs further investigation, an explanation solely

926 involving a tectonic hiatus during the Middle to Late Miocene is no longer
927 satisfactory.

928

929 **Conclusions**

930 The sedimentary record of the Ouarzazate foreland basin provides valuable insights
931 into the evolution of the adjacent intracontinental High Atlas Mountains. In this study,
932 lacustrine sequences at five locations representing a temporal transect from the
933 Middle to Late Miocene across the wider Ouarzazate Basin region were investigated.
934 Facies descriptions, thin-section analysis, and carbon and oxygen isotopes
935 measurements were undertaken focussing on the carbonate beds of the Middle to
936 Late Miocene Aït Kandoula Formation. Previous work by Benammi & Jaeger (2001),
937 Benammi et al. (1996) and Teson et al. (2010) provide the stratigraphic framework
938 and age constraints for the sedimentology and geochemistry undertaken in this
939 study. We demonstrate that these carbonates and palaeosols were indeed
940 deposited initially in a hydrologically closed foreland basin, as proposed by El Harfi et
941 al. (2001) and others but not previously unequivocally demonstrated. Furthermore,
942 the facies associations of the Serravallian to Tortonian are characteristic of
943 underfilled foreland basins with fluctuations between lacustrine highstands and
944 lowstands driving much of the sedimentological variation observed in the sections.
945 However, we also identify a previously unrecognised shift in the hydrodynamics of
946 the lake system to open conditions in the late Tortonian based upon carbon and
947 oxygen isotope covariance and corresponding to changes in the facies associations
948 to persistent lake facies. While further research is needed, the evidence presented
949 here indicates that these sediments were potentially deposited during a period of
950 continued subsidence in the basin with superimposed climatic trends. This
951 interpretation strongly suggests that this was not a period of tectonic quiescence but
952 rather that tectonic loading and therefore active thrusting were ongoing throughout
953 the Middle to Late Miocene. As such this formation records important evidence for
954 the long-term continuous uplift of the High Atlas Mountains, with implications for
955 geodynamic models of the evolution of this mountain chain and the wider western
956 Mediterranean region. The fine-grained nature of the succession and ability to
957 generate reliable magnetostratigraphic constraints on the timing of deposition also

958 indicates that these rocks could also be an excellent, but as yet untapped, archive of
959 Late Miocene climate change on the edge of the Sahara.

960

961 **Acknowledgements**

962 We thank the Royal Geographical Society with IGB for the award of the Thesiger-
963 Oman Fellowship to SB, which funded this research. Funding for JvV was provided
964 by Natural Environment Research Council (NERC) NE/J020842/1. We also thank
965 Martin Stokes and Jesse Zondervan for useful discussions that have improved the
966 manuscript. The SRTM 1 arcs data product was retrieved from the online Data Pool,
967 courtesy of the NASA Land Processes Distributed Active Archive Center (LP DAAC),
968 USGS/Earth Resources Observation and Science (EROS) Center, Sioux Falls,
969 South Dakota, https://lpdaac.usgs.gov/data_access/data_pool.

970

971 **References**

- 972 Alçiçek, H. and Alçiçek, M.C., (2014). Palustrine carbonates and pedogenic calcretes in the
973 Çal basin of SW Anatolia: Implications for the Plio-Pleistocene regional climatic pattern
974 in the eastern Mediterranean. *Catena*, 112, 48–55.
- 975 Allen, P.A., Armitage, J.J., Carter, A., Duller, R.A., Michael, N.A., Sinclair, H.D., Whitchurch,
976 A.L. and Whittaker, A.C. (2013). The Qs problem: sediment volumetric balance of
977 proximal foreland basin systems. *Sedimentology*, 60(1), 102-130.
- 978 Alonso-Zarza, A.M. (2003). Palaeoenvironmental significance of palustrine carbonates and
979 calcretes in the geological record. *Earth Science Reviews*, 60(3), 261-298.
- 980 Alonso-Zarza, A. M., Meléndez, A., Martín-García, R., Herrero, M. J. and Martín-Pérez, A.
981 (2012). Discriminating between tectonism and climate signatures in palustrine deposits:
982 Lessons from the Miocene of the Teruel Graben, NE Spain, *Earth-Science Reviews*.
983 Elsevier, 113(3–4), 141–160.
- 984 Arboleya, M.-L., Babault, J., Owen, L. A., Teixell, S. and Finkel, R. C. (2008) ‘Timing and
985 nature of Quaternary fluvial incision in the Ouarzazate foreland basin, Morocco, *Journal*
986 *of the Geological Society*, 165(6), 1059–1073.
- 987 Arenas, C. and Pardo, G. (1999). Latest Oligocene–Late Miocene lacustrine systems of the
988 north-central part of the Ebro Basin (Spain): sedimentary facies model and
989 palaeogeographic synthesis. *Palaeogeography, Palaeoclimatology, Palaeoecology*,
990 151(1–3), 127–148.

- 991 Armitage, J. J., Duller, R. A., Whittaker, A. C., and Allen, P. A. (2011). Transformation of
992 tectonic and climatic signals from source to sedimentary archive. *Nature Geoscience*,
993 4(4), 231.
- 994 Ashley, G.M., Bunn, H.T., Delaney, J.S., Barboni, D., Domínguez-Rodrigo, M., Mabulla, A.Z.,
995 Gurtov, A.N., Baluyot, R., Beverly, E.J. and Baquedano, E. (2014). Paleoclimatic and
996 paleoenvironmental framework of FLK North archaeological site, Olduvai Gorge,
997 Tanzania. *Quaternary International*, 322, 54-65.
- 998 Babault, J., Teixell, A., Arboleya, M. L., and Charroud, M. (2008). A late Cenozoic age for
999 long-wavelength surface uplift of the Atlas Mountains of Morocco. *Terra Nova*, 20(2),
1000 102–107.
- 1001 Balestrieri, M. L., Moratti, G., Bigazzi, G., and Algouti, A. (2009). Neogene exhumation of the
1002 Marrakech High Atlas (Morocco) recorded by apatite fission-track analysis. *Terra Nova*,
1003 21(2), 75–82.
- 1004 Barbero, L., Teixell, A., Arboleya, M. L., del Río, P., Reiners, P. W. and Bougadir, B. (2007).
1005 ‘Jurassic-to-present thermal history of the central High Atlas (Morocco) assessed by
1006 low-temperature thermochronology’, *Terra Nova*, 19(1), 58–64.
- 1007 Beauchamp, W., Allmendinger, R. W., Barazangi, M., Demnati, A., El Alji, M. and Dahmani,
1008 M. (1999). ‘Inversion tectonics and the evolution of the High Atlas Mountains, Morocco,
1009 based on a geological-geophysical transect’, *Tectonics*, 18(2), 163–184.
- 1010 Benammi, M., and Jaeger, J.-J. (2001). Magnetostratigraphy and palæontology of the
1011 continental Middle Miocene of the Aït Kandoula Basin, Morocco. *Journal of African Earth*
1012 *Sciences*, 33(2), 335–348.
- 1013 Benammi, M., Orth, B., Vianey-Liaud, M., Chaimanee, Y., Suteethorn, V., Feraud, G.,
1014 Hernandez, J. and Jaeger, J.J. (1995). Micromammifères et biochronologie des
1015 formations néogènes du flanc sud du Haut-Atlas Marocain: implications
1016 biogéographiques, stratigraphiques et tectoniques. *Africa Geoscience Review*,
1017 2(2), 279-310.
- 1018 Benammi, M., Calvo, M., Prévot, M., and Jaeger, J.-J. (1996). Magnetostratigraphy and
1019 paleontology of Aït Kandoula basin (High Atlas, Morocco) and the African-European late
1020 Miocene terrestrial fauna exchanges. *Earth and Planetary Science Letters*, 145(1–4),
1021 15–29.
- 1022 Bohacs, K. M. (1998). Contrasting expressions of depositional sequences in mudrocks from
1023 marine to non marine environs. In: Schrieber, J., Zimmerle, W., Sethi, P.S., (Eds)
1024 *Shales and Mudstones. Volume I, Basin studies, sedimentology, and paleontology.* 33-
1025 78.
- 1026 Bohacs, K.M., Carroll, A.R., Neal, J.E. and Mankiewicz, P.J. (2000). Lake-basin type, source
1027 potential, and hydrocarbon character: an integrated sequence-stratigraphic-geochemical

- 1028 framework. In: E. H. Gierlowski Kordesch and K. R. Kelts, (eds). Lake basins through
1029 space and time: AAPG Studies in Geology, 46, 3-34.
- 1030 Boulton, S.J., Stokes, M. and Mather, A.E. (2014). Transient fluvial incision as an indicator of
1031 active faulting and Plio-Quaternary uplift of the Moroccan High Atlas. *Tectonophysics*,
1032 633, 16-33.
- 1033 Burbank, D.W., (1992). Causes of recent Himalayan uplift deduced from deposited patterns
1034 in the Ganges basin. *Nature*, 357(6380), 680.
- 1035 Burbank, D.W. and Vergés, J. (1994). Reconstruction of topography and related depositional
1036 systems during active thrusting. *Journal of Geophysical Research: Solid Earth*, 99(B10),
1037 20281-20297.
- 1038 Burne, R.V. and Ferguson, J. (1983). Contrasting marginal sediments of a seasonally
1039 flooded saline lake—Lake Eliza, South Australia: significance for oil shale genesis.
1040 BMR, *Journal of Australian Geology and Geophysics*, 8, 99-108.
- 1041 Cabaleri, N.G. and Benavente, C.A. (2013). Sedimentology and paleoenvironments of the
1042 Las Chacritas carbonate paleolake, Cañadón Asfalto Formation (Jurassic), Patagonia,
1043 Argentina. *Sedimentary Geology*, 284, 91-105.
- 1044 Carrapa, B. and DeCelles, P.G. (2008). Eocene exhumation and basin development in the
1045 Puna of northwestern Argentina. *Tectonics*, 27(1).
- 1046 Carroll, A.R. and Bohacs, K.M. (1999). Stratigraphic classification of ancient lakes:
1047 Balancing tectonic and climatic controls. *Geology*, 27(2), 99-102.
- 1048 Cecil, C.B. (1990). Paleoclimate controls on stratigraphic repetition of chemical and
1049 siliciclastic rocks. *Geology*, 18(6), 533-536.
- 1050 Clevis, Q., de Boer, P. and Wachter, M., (2003). Numerical modelling of drainage basin
1051 evolution and three-dimensional alluvial fan stratigraphy. *Sedimentary Geology*, 163(1-
1052 2), 85-110.
- 1053 Cobbold, P.R., Zanella, A., Rodrigues, N. and Løseth, H. (2013). Bedding-parallel fibrous
1054 veins (beef and cone-in-cone): Worldwide occurrence and possible significance in terms
1055 of fluid overpressure, hydrocarbon generation and mineralization. *Marine and Petroleum*
1056 *Geology*, 43, 1-20.
- 1057 DeCelles, P.G., Gray, M.B., Ridgway, K.D., Cole, R.B., Srivastava, P., Pequera, N. and
1058 Pivnik, D.A. (1991). Kinematic history of a foreland uplift from Paleocene synorogenic
1059 conglomerate, Beartooth Range, Wyoming and Montana. *Bulletin of the Geological*
1060 *Society of America*, 103(11), 1458-1475.
- 1061 Densmore, A.L., Ellis, M.A., Li, Y., Zhou, R., Hancock, G.S. and Richardson, N. (2007).
1062 Active tectonics of the Beichuan and Pengguan faults at the eastern margin of the
1063 Tibetan Plateau. *Tectonics*, 26(4), TC4005.

- 1064 de Wet, C.B., Godfrey, L. & de Wet, A.P. (2015). Sedimentology and stable isotopes from a
1065 lacustrine-to-palustrine limestone deposited in an arid setting, climatic and tectonic
1066 factors: Miocene–Pliocene Opache Formation, Atacama Desert, Chile.
1067 *Palaeogeography, Palaeoclimatology, Palaeoecology*, 426, 46–67.
- 1068 Duller, R.A., Whittaker, A.C., Fedele, J.J., Springett, J., Smithells, R. and Allen, P.A. (2010)
1069 From grain size to tectonics. *Journal of Geophysical Research - Earth Surface*, 115,
1070 F03022.
- 1071 Dunagan, S.P. and Driese, S.G., 1999. Control of terrestrial stabilization on Late Devonian
1072 palustrine carbonate deposition; Catskill Magnafacies, New York, USA. *Journal of*
1073 *Sedimentary Research*, 69(3), 772-783.
- 1074 Dunagan, S.P. and Turner, C.E., (2004). Regional paleohydrologic and paleoclimatic
1075 settings of wetland/lacustrine depositional systems in the Morrison Formation (Upper
1076 Jurassic), Western Interior, USA. *Sedimentary Geology*, 167(3), 269-296.
- 1077 Dunham, R. J. (1962). Classification of carbonate rocks according to depositional textures: in
1078 Ham, W.E., ed., *Classification of Carbonate Rocks*. American Association of Petroleum
1079 Geologists, Memoir 1, 108-121.
- 1080 El Harfi, A., Lang, J., Salomon, J., and Chellai, E. H., (2001). Cenozoic sedimentary
1081 dynamics of the Ouarzazate foreland basin (central High Atlas Mountains,
1082 Morocco). *International Journal of Earth Sciences*, 90, 393-411.
- 1083 El Harfi, A., Guiraud, M. & Lang, J., (2006). Deep-rooted “thick skinned” model for the High
1084 Atlas Mountains (Morocco). Implications for the structural inheritance of the southern
1085 Tethys passive margin. *Journal of Structural Geology*, 28(11), 1958–1976.
- 1086 Flemings, P.B. and Jordan, T.E., (1990). Stratigraphic modeling of foreland basins:
1087 Interpreting thrust deformation and lithosphere rheology. *Geology*, 18(5), 430-434.
- 1088 Flugel, E., (2004). *Microfacies of carbonate rocks: analysis, interpretation and application*.
1089 Springer.
- 1090 Fraissinet, C., El Zouine, M., Morel, J.L., Poisson, A., Andrieux, J. and Faure-Muret, A.,
1091 (1988). Structural evolution of the southern and northern central High Atlas in
1092 Paleogene and Mio-Pliocene times. In: *The Atlas System of Morocco*. Springer Berlin
1093 Heidelberg, 273 – 291.
- 1094 Freytet, P., (1971). Paléosols résiduels et paléosols alluviaux hydromorphes dans le Crétacé
1095 supérieur et l'Eocène basal en Languedoc. *Revue Géographie Physic Géologie*
1096 *Dynamique*. XIII: 245–268.
- 1097 Freytet, P., (1973). Petrography and paleo-environment of continental carbonate deposits
1098 with particular reference to the Upper Cretaceous and Lower Eocene of Languedoc
1099 (Southern France). *Sedimentary Geology*, 10(1), 25-60.

- 1100 Freytet, P., (1984). Les sédiments lacustres carbonatés et leur transformation par émergence
1101 et pédogénèse. Importance de leur identification pour les reconstitutions
1102 paléogéographiques. Bulletin des Centres de Recherche et Exploration-Production Elf-
1103 Aquitaine, 8: 223–247.
- 1104 Freytet, P. and Verrecchia, E.P., (2002). Lacustrine and palustrine carbonate petrography:
1105 an overview. *Journal of Paleolimnology*, 27(2), 221-237.
- 1106 Fraissinet, de F., Saint Bezar, B., Bracène, R. and Mercier, E., (2000). The two main steps
1107 of the Atlas building and geodynamics of the western Mediterranean. *Tectonics*, 19(4),
1108 740-761.
- 1109 Frizon de Lamotte, D., Saint Bezar, B., Bracène, R. and Mercier, E., (2000). The two main
1110 steps of the Atlas building and geodynamics of the western Mediterranean. *Tectonics*,
1111 19(4), 740-761.
- 1112 Frizon de Lamotte, D., Leturmy, P., Missenard, Y., Khomsi, S., Ruiz, G., Saddiqi, O.,
1113 Guillocheau, F. and Michard, A. (2009), Mesozoic and Cenozoic vertical movements in
1114 the Atlas system (Algeria, Morocco, Tunisia): An overview. *Tectonophysics*, 475(1), 9–
1115 28.
- 1116 Görler, K., Helmdach, F.F., Gaemers, P., Heissig, K., Hinsch, W., Mädler, K., Shwarzans,
1117 W., and Zucht, M., (1988). The uplift of the central High Atlas as deduced from Neogene
1118 continental sediments of the Ouarzazate province, Morocco. *Lecture Notes in Earth
1119 Science*, 15, 363–404.
- 1120 Gomez, F., Beauchamp, W. and Barazangi, M., (2000). Role of the Atlas Mountains
1121 (northwest Africa) within the African-Eurasian plate-boundary zone. *Geology*, 28(9),
1122 775–778.
- 1123 Goudie, A.S., (1996). Organic agency in calcrete development. *Journal of Arid
1124 Environments*, 32(2), pp.103–110.
- 1125 Gradstein, F. M., Ogg, J. G., Schmitz, M. and Ogg, G. (Eds.). (2012). *The geologic time
1126 scale 2012*. Elsevier, New York. Accessed through the Timescale Creator website
1127 <https://engineering.purdue.edu/Stratigraphy/tscreator/index/index.php>.
- 1128 Heller, P.L., Angevine, C.L., Winslow, N.S. and Paola, C., (1988). Two-phase stratigraphic
1129 model of foreland-basin sequences. *Geology*, 16(6), 501-504.
- 1130 Herdendorf, C.E., (1984). Inventory of the morphometric and limnologic characteristics of the
1131 large lakes of the world. The Ohio State University Sea Grant Program, Technical
1132 Bulletin OHSU-TB-17, 78 p.
- 1133 Jacobshagen, V., Görler, K. and Giese, P., (1988). Geodynamic evolution of the Atlas
1134 System (Morocco) in post-Palaeozoic times. In: *The Atlas System of Morocco*. Springer
1135 Berlin Heidelberg, 481-499.

- 1136 Jaeger, J-J., (1977). Les Rongeurs du Miocène moyen et supérieur du Maghreb.
1137 *Palaeovertebrata*, 8 (1), 1–166
- 1138 Keith, M.L. and Weber, J.N., (1964). Carbon and oxygen isotopic composition of selected
1139 limestones and fossils. *Geochimica et Cosmochimica Acta*, 28(10),1787-1816.
- 1140 Leprêtre, R., Missenard, Y., Saint-Bezar, B., Barbarand, J., Delpech, G., Yans, J.,
1141 Dekoninck, A. and Saddiqi, O. (2015), The three main steps of the Marrakech High Atlas
1142 building in Morocco: Structural evidences from the southern foreland, Imini area, *Journal*
1143 *of African Earth Sciences*. Pergamon, 109, 177–194.
- 1144 Marr, J. G., Swenson, J. B., Paola, C., and Voller, V. R. (2000). A two-diffusion model of
1145 fluvial stratigraphy in closed depositional basins. *Basin Research*, 12(3-4), 381-398.
- 1146 Missenard, Y., Zeyen, H., de Lamotte, D. F., Leturmy, P., Petit, C., Sébrier, M. and Saddiqi,
1147 O. (2006) Crustal versus asthenospheric origin of relief of the Atlas mountains of
1148 Morocco, *Journal of Geophysical Research: Solid Earth*, 111(3), 1–13.
- 1149 Parsons, A.J., Michael, N.A., Whittaker, A.C., Duller, R.A. and Allen, P.A. (2012) Grain - size
1150 trends reveal the late orogenic tectonic and erosional history of the south - central
1151 Pyrenees, Spain. *Journal of the Geological Society, London*, 169, 111 - 114.
- 1152 Pastor, À., Teixell, A. and Arboleya, M.L., (2012). Rates of quaternary deformation in the
1153 ouarzazate basin (southern atlas front, Morocco). *Annals of Geophysics*, 55(5), 1003–
1154 1016.
- 1155 Pietras, J.T., Carroll, A.R. and Rhodes, M.K., (2003). Tectonic control on lacustrine evaporite
1156 deposition in the Eocene Green River Formation. Wyoming. *Journal of Paleolimnology*,
1157 70, 115-125.
- 1158 Platt, N. H. and Wright, V.P., (1991). Lacustrine carbonates: facies models, facies
1159 distribution and hydrocarbon aspects. In: Anadon, P., L. Cabrera & K. Kelts (eds),
1160 *Lacustrine Facies Analysis*. IAS special publication 13. Blackwell, Oxford, 57–74.
- 1161 Platt, N.H. and Wright, V.P., (1992). Palustrine Carbonates and the Florida Everglades:
1162 towards an exposure index for the fresh-water environment? *Journal of Sedimentary*
1163 *Research*, 62(6), 1058-1071.
- 1164 Pla-Pueyo, S., Gierlowski-Kordesch, E.H., Viseras, C. and Soria, J.M., (2009). Major
1165 controls on sedimentation during the evolution of a continental basin: Pliocene–
1166 Pleistocene of the Guadix Basin (Betic Cordillera, southern Spain). *Sedimentary*
1167 *Geology*, 219(1-4), 97-114.
- 1168 Potter, P.E. and Szatmari, P., (2009). Global Miocene tectonics and the modern world. *Earth*
1169 *Science Reviews*, 96(4), 279-295.

- 1170 Remy, J-A., Benammi, M., (2006). Presence of a Gomphotheriidea indet. (Proboscidea,
1171 Mammalia) in the Vallesian fauna of Afoud AF6 (Aït Kandoula Basin, Morocco), inferred
1172 from the enamel microstructure of a molar chip. *Geobios*, 555-562.
- 1173 Roehler, H.W., (1993). Eocene climates, depositional environments, and geography, greater
1174 Green River Basin, Wyoming, Utah, and Colorado. United States Geological Survey,
1175 Professional Paper, (1506-F).
- 1176 Sáez, A., Anadón, P., Herrero, M.J. and Moscariello, A., (2007). Variable style of transition
1177 between Palaeogene fluvial fan and lacustrine systems, southern Pyrenean foreland,
1178 NE Spain. *Sedimentology*, 54(2), 367-390.
- 1179 Schuster, M., Durringer, P., Ghiene, J.F., Vignaud, P., Mackaye, H.T., Likius, A. and Brunet,
1180 M., (2006). The age of the Sahara desert. *Science*, 311, 821-821.
- 1181 Sepulchre, P., Ramstein, G., Fluteau, F., Schuster, M., Tiercelin, J.J. and Brunet, M., (2006).
1182 Tectonic uplift and Eastern Africa aridification. *Science*, 313, 1419-1423.
- 1183 Stäblein, G., (1988). Geomorphological aspects of the Quaternary evolution of the
1184 Ouarzazate Basin, Southern Morocco: *Lecture Notes in Earth Sciences*, 15, 433–443.
- 1185 Stokes, M., Mather, A. E., Belfoul, A. and Farik, F. (2008), Active and passive tectonic
1186 controls for transverse drainage and river gorge development in a collisional mountain
1187 belt (Dades Gorges, High Atlas Mountains, Morocco), *Geomorphology*, 102(1), 2–20.
- 1188 Stokes, M., Mather, A. E., Belfoul, M., Faik, F., Bouzid, S., Geach, M. R., Cunha, P. P.,
1189 Boulton, S. J. and Thiel, C. (2017) Controls on dryland mountain landscape
1190 development along the NW Saharan desert margin: Insights from Quaternary river
1191 terrace sequences (Dadès River, south-central High Atlas, Morocco), *Quaternary*
1192 *Science Reviews*, 166, 363, 379.
- 1193 Talbot, M.R., (1990). A review of the palaeohydrological interpretation of carbon and oxygen
1194 isotopic ratios in primary lacustrine carbonates. *Chemical Geology*, 80(4), 261-279.
- 1195 Talbot, M. R., and Kelts, K., (1990). Paleolimnological Signatures from Carbon and Oxygen
1196 Isotopic Ratios in Carbonates. In: B.J. Katz, B.R. Rosendahl (Eds.), *Lacustrine Basin*
1197 *Exploration: Case Studies and Modern Analogs*. AAPG Special Volume, M50, 99-112.
- 1198 Tanner, L.H., (2000). Miocene-Pliocene Lacustrine and Marginal Lacustrine Sequences of
1199 the Furnace Creek Formation, Furnace Creek and Central Death Valley Basins, Death
1200 Valley Region, USA. *AAPG Studies in Geology*# 46, Chapter 44 481-489.
- 1201 Teson, E. and Teixell, A., (2008), Sequence of thrusting and syntectonic sedimentation in
1202 the eastern sub-Atlas thrust belt (Dades and Mgoun valleys, Morocco). *International*
1203 *Journal of Earth Science*, 97, 103–113.
- 1204 Teson, E., Puyoe, E.L., Teixell, A., Barnolas, A., Agustí, J., and Furio, M., (2010).
1205 *Magnetostratigraphy of the Ouarzazate Basin: Implications for the timing of deformation*

- 1206 and mountain building in the High Atlas Mountains of Morocco. *Geodinamica Acta*, 23,
1207 151-165.
- 1208 Valero-Garcés, B.L. and Aguilar, J.G., (1992). Shallow carbonate lacustrine facies models in
1209 the Permian of the Aragon-Bearn basin (Western Spanish-French Pyrenees).
1210 *Carbonates Evaporites*, 7(2), 94-107.
- 1211 Valero-Garcés, B.L., Kelts, K. and Ito, E., (1995). Oxygen and carbon isotope trends and
1212 sedimentological evolution of a meromictic and saline lacustrine system: the Holocene
1213 Medicine Lake basin, North American Great Plains, USA. *Palaeogeography,*
1214 *Palaeoclimatology, Palaeoecology*, 117(3), 253-278.
- 1215 Whittaker, A.C., Duller, R.A., Springett, J., Smithells, R., Whitchurch, A.L. and Allen, P.A.
1216 (2011) Decoding downstream trends in stratigraphic grain - size as a function of tectonic
1217 subsidence and sediment supply. *Bulletin of the Geological Society America*, 123,
1218 1363 - 1382.
- 1219 Wright, V.P. (1990). A micromorphological classification of fossil and recent calcic and
1220 petrocalcic microstructures. *Developments in soil science*, 19, 401-407.
- 1221 Wright, V.P. and Platt, N.H., (1995). Seasonal wetland carbonate sequences and dynamic
1222 catenas: a re-appraisal of palustrine limestones. *Sedimentary Geology*, 99(2), 65-71.
- 1223 Wright, V.P., Platt, N.H., Marriott, S.B. and Beck, V.H. (1995). A classification of rhizogenic
1224 (root-formed) calcretes, with examples from the Upper Jurassic-Lower Cretaceous of
1225 Spain and Upper Cretaceous of southern France. *Sedimentary Geology*, 100(1), 143-
1226 158.
- 1227 Zouhri, S., Geraads, D., El Boughabi, S. and El Harfi, A. (2012), Discovery of an Upper
1228 Miocene Vertebrate fauna near Tizi N'Tadderht, Skoura, Ouarzazate Basin (Central
1229 High Atlas, Morocco), *Comptes Rendus Palevol*. 11(6), 455–461.
- 1230
- 1231
- 1232

Facies code		Facies Name	Description	Process	Interpretation
Mp	1	Mottled mudstone	Red to grey/white mottled mudstones, occasionally gypsiferous, occasional caliche nodules and root traces.	Soil formation	Paleosols forming in flood plain or marginal lacustrine environments.
M	2	Mudstone	Thin beds (< 5 cm) of dark grey to black mudstone, rich in microfossil material.	Settling from suspension, low oxygen conditions	Basin deposition
Ma	3	Marl	Thick beds of massive light grey marl, variable fossil content, locally gypsiferous.	Settling from suspension	Basin deposition
Sp	4	Planar laminated sandstone	Very coarse-grained to granular litharenite with planar laminations. Bedding planes are sharp and beds are 0.25 – 0.5 m thick.	Upper flow regime laminar flow	Flood deposition
Sch	5	Channelised granular to pebbly sandstones	Granular to pebbly litharenites, generally have sharp, erosional bases forming wide and shallow channel structures.	Sediment infilling channel scours	Small fluvial channels.
Gy	6	Selenite Gypsum	Selenite gypsum crystals up to 5 cm in length	Subaqueous crystallisation from brine	Evaporitic conditions
Gf	7	Fibrous Gypsum			
Sg	8	Gypsarenite	White, very fine-grained, well sorted gypsum sandstone.	Accumulation of detrital gypsum	Evaporiate shaol/flat
Gg	9	Gypsiferous conglomerate	Matrix supported conglomerate formed of selenite crystals up to 30 cm in length in a pink – red lime mudstone matrix.	Debris flow	Downslope transport.
Gc	10	Clast-supported conglomerate	Clast-supported conglomerate with sub-angular to rounded, poorly sorted clasts of various lithologies. Beds are laterally continuous with sharp, locally erosional bases.	Sheet flood	Distal alluvial fan
LM	11	Carbonates	Thinly bedded mudstones and packstones with	Settling from suspension or	Lacustrine

gastropods and bioclastic fragments. Beds are sharp and often laterally discontinuous. Bioturbation is common, where absent algal laminations are present. accumulation in algal mats. Subsequent pedogenic alteration

1233

1234 Table 1. Summary of sedimentary facies

1235

1236 Table 2. Stable isotope data.

Section 01				
Sample ID	d ¹³ C	d ¹⁸ O	Section height (m)	Facies
MR0101	-5.83	-7.32	10.35	1
MR0103	-5.84	-8.35	49.95	1
MR0104A	-6.58	-8.10	50.65	2
MR0104B	-6.65	-6.91	50.65	2
MR0105	-6.00	-7.66	60.65	2
MR0106	-6.14	-7.76	61.15	2
MR0107	-5.93	-7.74	61.65	2
MR0108A	-6.42	-7.79	65.65	2
MR0108B	-6.44	-7.80	65.65	2
MR0109	-5.96	-7.57	66.55	2
MR0110	-6.63	-8.65	67.05	2
MR0111	-6.49	-7.89	69.75	1
MR0112	-6.97	-7.93	75.1	2
MR0113	-6.81	-7.98	80.4	2
MR0114	-6.55	-7.92	80.85	2
MR0115	-6.21	-8.54	82.85	2
MR0116	-6.31	-8.44	87.75	2
MR0117A	-6.19	-8.79	90.45	1
MR0117B	-6.43	-8.89	90.45	1
MR0118A	-6.40	-8.31	91.45	1
MR0118B	-6.81	-8.62	91.45	1
MR0119	-6.82	-8.01	95.05	1

Carbonates of the Ouarzazate Basin.

MR0120	-7.28	-8.93	96.75	2
MR0121	-6.92	-8.34	97.95	2
MR0122	-6.03	-7.89	102.45	2
MR0123	-5.88	-7.62	103.25	2
Section 02				
MR0201	-4.61	-7.19	4.50	1
MR0202	-5.73	-8.17	5.00	1
MR0203	-5.66	-8.71	5.25	1
MR0205	-8.12	-9.63	7.80	1
MR0206	-5.18	-7.89	78.84	1
MR0209	-5.61	-8.01	204.79	1
MR0211	-4.14	-5.16	355.18	1
MR0212	-6.39	-8.78	357.48	1
Section 04				
MR4A01	-4.92	1.17	0.90	1
MR4A04	-6.27	-4.00	2.40	3
MR4A05	-5.70	-6.61	2.60	3
MR0402	-5.55	-5.76	4.30	1
MR0403	-5.54	-6.21	4.70	1
MR0404	-5.83	-6.70	5.40	1
MR0405	-5.50	-6.45	5.70	1
MR0406	-4.93	-6.33	6.00	1
MR0407	-5.97	-6.02	8.80	1
MR0408	-6.68	-5.90	9.10	1
MR0409	-6.41	-5.40	9.22	1
MR0410	-5.77	-5.70	9.67	1
MR0411	-4.99	-3.81	9.82	1
MR0414	-7.57	-6.54	11.72	1
MR0415	-6.11	-6.18	13.97	3
MR0416	-5.46	-6.39	14.17	3
MR0419	-6.87	-6.98	25.32	1
MR0420	-7.65	-6.83	26.72	3
MR0422	-7.69	-8.17	27.02	1
MR0424	-7.01	-7.57	27.57	1
MR0425	-5.45	-8.36	35.32	1

Carbonates of the Ouarzazate Basin.

MR0426	-5.83	-6.45	39.42	3
MR0427	-6.07	-6.08	40.52	1
MR0428	-5.48	-5.92	41.27	1
MR0430	-5.71	-6.98	51.52	1
MR0431	-5.46	-7.77	51.82	1
Section 05				
MR0502	-3.03	-7.59	4.7	1
MR0503	-3.92	-7.92	8.75	1
MR0504	-3.55	-8.42	9.25	1
MR0505	-3.51	-5.87	12.55	1
MR5A02	-4.56	-8.26	45	1
MR5A03	-4.39	-7.39	45.25	1
Section 06				
MR0601A	-5.02	-3.73	12	1
MR0601B	-4.17	-3.70	12	1
MR0602	-5.20	-2.81	20.5	1
MR0603	-5.16	-3.36	25	1
MR0604	-4.39	-1.91	54.25	1
MR0605	-4.02	-1.96	54.75	1a
MR0606	-4.47	-2.11	55.75	1
MR0607	-5.24	-4.65	56.25	1
MR0608	-5.16	-4.06	56.75	1
MR0609	-5.09	-3.20	57.25	1
MR0610	-5.59	-4.34	57.75	1
MR0611	-4.39	-3.20	58.25	1a
MR0612	-4.79	-4.38	58.75	1a
MR0613	-4.61	-3.21	59.25	1a
MR0614	-5.48	-3.69	59.75	1a
MR0615	-6.72	-6.12	61.5	1
MR0616	-6.57	-6.04	68.25	1
MR0617	-5.89	-5.12	68.75	1
MR0618	-6.85	-5.55	69.25	1
MR0619	-6.84	-6.48	69.5	1a
MR0620	-5.98	-4.90	73	1a
MR0621	-5.59	-2.47	76.5	1

Carbonates of the Ouarzazate Basin.

MR0622	-6.08	-5.98	80	1
MR0623	-7.38	-7.36	80.5	1a
MR0624	-7.71	-7.60	81.5	1
MR0625	-6.09	-6.48	83	1
MR0626A	-6.19	-7.27	83.5	1
MR0626B	-5.99	-6.89	83.5	1
MR0627	-6.77	-7.06	84.5	1
MR0628	-6.57	-7.16	85	1
MR0629	-6.80	-7.99	87.25	1
MR0630	-7.09	-7.43	88	1
MR0631	-6.99	-7.46	88.75	1
MR0633	-6.61	-6.72	91.5	1
MR0634	-3.07	-6.51	92.75	2
MR0635	-5.93	-6.52	97	2
MR0636	-6.62	-7.18	98.25	2
MR0637	-6.15	-8.35	102.75	2
MR0638	-6.67	-8.25	103.75	2
MR0639	-5.74	-7.54	104.1	1
MR0640	-5.06	-6.73	104.15	2
MR0641	-6.13	-7.24	104.7	2
MR0642	-5.87	-7.52	105.05	2
MR0643	-5.44	-7.70	105.2	2
MR0644	-5.76	-7.11	105.3	2
MR0645	-5.53	-6.80	105.7	2
MR0646	-6.21	-7.95	106.2	2
MR0647	-4.29	-4.12	127.8	1
MR0648	-5.17	-1.18	129.3	1
MR0649	-2.12	-2.34	132.95	1
MR0650	-5.82	-8.27	146.2	1
MR0652	-5.84	-8.93	151.45	1
MR0653	-4.47	-8.51	152.2	1
MR0654	-5.47	-8.38	157.2	1